

1987

Studies on the mechanism of ethylene hydrogenation over iridium (111) single crystals

James Thomas Lloyd
Iowa State University

Follow this and additional works at: <https://lib.dr.iastate.edu/rtd>

 Part of the [Physical Chemistry Commons](#)

Recommended Citation

Lloyd, James Thomas, "Studies on the mechanism of ethylene hydrogenation over iridium (111) single crystals " (1987). *Retrospective Theses and Dissertations*. 11704.
<https://lib.dr.iastate.edu/rtd/11704>

This Dissertation is brought to you for free and open access by the Iowa State University Capstones, Theses and Dissertations at Iowa State University Digital Repository. It has been accepted for inclusion in Retrospective Theses and Dissertations by an authorized administrator of Iowa State University Digital Repository. For more information, please contact digirep@iastate.edu.

INFORMATION TO USERS

While the most advanced technology has been used to photograph and reproduce this manuscript, the quality of the reproduction is heavily dependent upon the quality of the material submitted. For example:

- Manuscript pages may have indistinct print. In such cases, the best available copy has been filmed.
- Manuscripts may not always be complete. In such cases, a note will indicate that it is not possible to obtain missing pages.
- Copyrighted material may have been removed from the manuscript. In such cases, a note will indicate the deletion.

Oversize materials (e.g., maps, drawings, and charts) are photographed by sectioning the original, beginning at the upper left-hand corner and continuing from left to right in equal sections with small overlaps. Each oversize page is also filmed as one exposure and is available, for an additional charge, as a standard 35mm slide or as a 17"x 23" black and white photographic print.

Most photographs reproduce acceptably on positive microfilm or microfiche but lack the clarity on xerographic copies made from the microfilm. For an additional charge, 35mm slides of 6"x 9" black and white photographic prints are available for any photographs or illustrations that cannot be reproduced satisfactorily by xerography.



Order Number 8721906

**Studies on the mechanism of ethylene hydrogenation over
iridium (111) single crystals**

Lloyd, James Thomas, Ph.D.

Iowa State University, 1987

U·M·I
300 N. Zeeb Rd.
Ann Arbor, MI 48106



PLEASE NOTE:

In all cases this material has been filmed in the best possible way from the available copy. Problems encountered with this document have been identified here with a check mark ✓.

1. Glossy photographs or pages _____
2. Colored illustrations, paper or print _____
3. Photographs with dark background ✓
4. Illustrations are poor copy _____
5. Pages with black marks, not original copy _____
6. Print shows through as there is text on both sides of page _____
7. Indistinct, broken or small print on several pages ✓
8. Print exceeds margin requirements _____
9. Tightly bound copy with print lost in spine _____
10. Computer printout pages with indistinct print _____
11. Page(s) _____ lacking when material received, and not available from school or author.
12. Page(s) _____ seem to be missing in numbering only as text follows.
13. Two pages numbered _____. Text follows.
14. Curling and wrinkled pages _____
15. Dissertation contains pages with print at a slant, filmed as received _____
16. Other _____

University
Microfilms
International



**Studies on the mechanism
of
ethylene hydrogenation
over iridium (111) single crystals**

by

James Thomas Lloyd

**A Dissertation Submitted to the
Graduate Faculty in Partial Fulfillment of the
Requirements for the Degree of
DOCTOR OF PHILOSOPHY**

Department: Chemistry

Major: Physical Chemistry

Approved:

Signature was redacted for privacy.

In Charge of Major Work

Signature was redacted for privacy.

For the Major Department

Signature was redacted for privacy.

For the Graduate College

**Iowa State University
Ames, Iowa**

1987

TABLE OF CONTENTS

	Page
INTRODUCTION	1
LITERATURE REVIEW	5
Ethylene Adsorption	5
Platinum	9
Other Metals	14
Nickel	16
Iridium	17
Kinetics	20
EXPERIMENTAL	37
Kinetic Procedures	37
Crystal Preparation	44
Sample Cleaning Procedures	47
Auger Electron Spectroscopy	48
Thermal Dehydrogenation Spectroscopy	51
RESULTS AND DISCUSSION	63
Hydrogen Dependence	63
Ethylene Dependence	66
Effect of Oxygen	70
Temperature Dependence	70
Auger Results	72
Temperature Dehydrogenation Spectroscopy	73
SUMMARY	103
REFERENCES	107
APPENDIX	114

INTRODUCTION

The oil-processing industry relies heavily on the ability of certain metals to catalyze a variety of reactions which alter the composition of their feedstocks to give them a more profitable mixture of hydrocarbons. Platinum has been the metal of choice for the catalyst of this process. Practical catalysts consist of finely divided metal particles on an oxide support. These practical catalysts can operate for thousands of hours without deactivation even though they are completely covered instantly with a hydrocarbon overlayer upon startup. The many reactions which occur in the reactor seem to be influenced very little by this hydrocarbon overlayer. The temperature of the reactor must be continually adjusted to keep the distribution of hydrocarbon products in a profitable region. Raising the temperature keeps the activity high but eventually leads to complete coverage of the catalyst with an inactive carbon overlayer. This process is known as coking. When the catalyst is completely coked, the reactor is shut down and the carbonaceous layer burned-off, regenerating the metal catalyst. It is beneficial to lengthen the period of time between reactor shutdowns for catalyst regeneration. Bimetallic catalysts have longer recycle times than the pure platinum catalysts. The most popular bimetallics are Pt-Re, Pt-Ir and Pt-Sn. The exact

role of the second metal in these platinum bimetallics is not well understood. The second metal in the bimetallics always has a greater ability to hydrogenate small hydrocarbon fragments. This property is beneficial in keeping the catalyst clear of harmful carbon deposits which can lead to coking. Until recently the vast majority of research in metal catalyzed hydrocarbon reactions has involved platinum or nickel and very little work has been done with the other metals.

Hydrocarbon reactions are sensitive to the conditions of pressure and temperature. To accurately characterize the kinetics of the reactions a broad range of pressures must be utilized. At very low pressures the overlayer structure does not develop under reaction conditions; at higher pressures, where the overlayer structure becomes evident, surface science techniques which demand high vacuum suffer. In the pressure regime where carbon deposits exist, the carbon overlayer can not be characterized.

To determine the reaction kinetics and the role the carbonaceous overlayer plays, a continuously stirred batch reactor was interfaced to an ultra-high-vacuum analysis chamber. Reaction kinetics and surface analysis are performed in one instrument.

The catalytic reaction is monitored to determine the kinetics under a variety of conditions. The temperature of

the catalyst and the partial pressures of the reactants can be varied over a very wide range. The metal catalyst can be analyzed before and after a kinetic trial to determine any changes in the chemical makeup of the surface.

To narrow the problem down to a reasonable size, simplifications are made. It is best to study the kinetics on a reaction where only one product is created over a well characterized surface. Ethylene hydrogenation should give only one product over iridium, ethane. Iridium was an obvious choice because of the lack of research on this important metal which is used in a significant number of reforming catalysts. The Auger spectrum nicely resolves the carbon peak from the metal peaks unlike the case with other metals used as reforming catalysts. The use of single crystals eliminates the effects mixed crystal orientation or catalyst geometry may have on the reaction. Ethylene hydrogenation was one of the first reactions to show catalytic behaviour. Even with its long history, its mechanism is still being studied and discussed. The number of reported mechanisms almost match the number of studies, but unfortunately none has proven to be significantly better or more popular than the others. Recently more attention has been given to the nature of the carbonaceous residue during the reaction.

Features of ethylene hydrogenation

- Very different mechanisms can represent experimental data equally well.
- The hydrogenation rate depends on catalyst pretreatment and conditions during the reaction.
- Unlike most catalytic reactions, the variations of the activation energy are small.
- Dispersion or metal particle size does not affect the rate.
- The reaction rate per unit area is nearly the same whether the metal is in powder, film, or single crystal form.
- Ethylene can react on the surface without hydrogen to give ethane.
- Ethylene is quite stably adsorbed on most metals.
- For as long as this catalytic reaction has been known, correlations between the hydrogenation activity and almost any known quantity (measured, calculated and dreamed-up) have been tried.
- Activity of alloy catalysts varies smoothly with alloy composition, indicating little or no sensitivity to the electronic structure of the metal.

LITERATURE REVIEW

Ethylene Adsorption

Ethylene adsorbs on metal surfaces in many ways. The complexity of ethylene adsorption is due to the ability of its bonds to rearrange to a variety of structures. Davis and Somorjai [1] have classified hydrocarbon adsorption by temperature into three regions:

1. Below room temperature.
Reversible adsorption of hydrocarbons.
Clean metal surfaces at high hydrogen pressures.
2. Above 700K.
Multilayer carbon buildup.
Poisoning by graphitic coke.
3. Temperatures below 700K and above room temperature.
Irreversible adsorption with sequential bond breaking and skeletal rearrangement.
Catalysis by active C_xH_y fragments at high hydrogen pressures.

These three temperature regions are not only divided by the types of ethylene derived species existing on the surface but also by the methodology used by experimentalists to probe the interaction of hydrocarbons with metal surfaces. Region one has been the domain of ultra-high-vacuum scientists with a few kinetic experiments being done. The bulk of the information on the low temperature states has

profited from the many surface sensitive vacuum probes. The second region has received very little attention in the literature except for a few papers dealing with poisoning or graphite deposition. The third region is the most profitable and complex region. A great deal of information is obtained directly and indirectly under a variety of conditions in this temperature regime.

The low temperature chemisorbed ethylene species have been probed extensively by a number of surface spectroscopies [2]. Species on the various crystal faces of platinum have received most extensive study, and the following discussion, to the extent numerical values are given, most accurately applies to platinum; studies of ethylene species on metals of the platinum group and related groups in the periodic table have been less extensive but results have been qualitatively similar to those for platinum. In subsequent sections results for specific metals, especially platinum and iridium, will be compared. At very low temperatures (below 200K) ethylene adsorbs associatively on some metals in the form of a π -bonded molecular complex oriented parallel to the surface. Pi-donation to the metal and back donation to the π^* orbital stabilizes the adsorbed ethylene and both effects contribute to the C-C bond stretching. The π -bonded species undergoes the minimum amount of structural and electronic deformation

as compared to the free molecule gas-phase ethylene. The valence band features present in ultra-violet photoelectron (UPS) spectra undergo several characteristic chemical shifts indicative of π -bonding to the metal surface [3]. The small chemical shifts for the chemisorbed molecule relative to the gas phase in the $1b_{2u}$, $3a_g$ and $1b_{1g}$ (σ) orbitals point to small electronic changes, but the $1b_{1u}$ (π) orbital moves down in energy by about 1 eV clearly pointing to π -bonded ethylene. High resolution electron energy loss spectroscopy (HREELS) is used as a vibrational fingerprint technique to solve for the adsorbate structures [4]. The HREELS spectrum characteristic of ethylene gives a strong feature around 990 cm^{-1} due to the CH_2 out-of-plane bend for an ethylene molecule oriented parallel to the surface and other weak features for π -bonded ethylene.

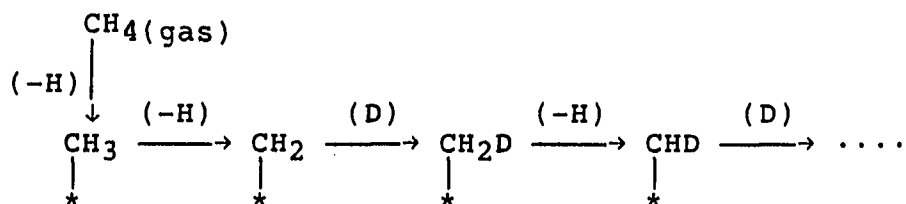
At higher temperatures the π -complex will transform into a di- σ -bonded associatively adsorbed ethylene species oriented parallel to the surface [2]. The UPS spectra record larger chemical shifts from the gas phase. The HREELS spectra, instead of appearing like a slightly modified gas phase ethylene spectra, resembles the sp^3 hybridized dibromoethane.

In the second temperature regime of Davis and Somorjai, many different and more strongly altered ethylene derived adsorbed species have been postulated. Bond rearrangements,

partial dehydrogenation and carbon-metal multiple bonds occur at temperatures above 250K. The chemistry in this temperature region is very rich for such a simple system [5]. Figure 1 shows a partial listing of the variety of configurations proposed for a partially hydrogenated two-carbon adsorbate. Many of these species have been given roles as intermediates in ethylene hydrogenation. The complexity of the various possible mechanisms is not diminished by the inclusion of the low temperature species, π -bonded and di- σ -bonded states, which are still populated at the temperatures and ethylene partial pressures commonly used in kinetic studies [6]. The metal surface is populated with a complex mixture of adspecies, part of which have some role in the hydrogenation of ethylene to ethane. The question of which of these various species participate and their relative importance in the hydrogenation mechanism is indeed a difficult challenge.

Scission of the C-H bonds occurs readily around 300K but still higher temperatures are necessary to break the C-C bond [7]. Monocarbon units form above 375K as evidenced by the evolution of hydrogen in the thermal desorption spectra and the onset of appreciable hydrogenolysis on the active metals. In the presence of hydrogen, the partially hydrogenated monocarbon species are easily completely hydrogenated to methane [8]. The ease of hydrogenation of

these monocarbon species is exemplified by the deuteration of methane. Kemball [9] proposed a correlation between hydrogenolysis activity and the ability of metals to form multiple bonds to hydrocarbons. To illustrate his point, he suggested the use of the deuterium-product distribution of methane-deuterium exchange as a diagnostic tool for multiple bond formation. A random or binomial distribution is expected from σ -monoadsorbed species. In his experiments, he found the distribution for the more active metals to be peaked about CHD_3 and CD_4 for which he suggested this mechanism,



The ease of deuteration of the partially dehydrogenated monocarbon species indicates they will be easily removed if formed in the presence of hydrogen.

Platinum

As mentioned previously the most popular metal in hydrocarbon catalysis is platinum and it deserves a more careful discussion of its interactions with ethylene. Much of what is known about the interaction of ethylene with metal surfaces is derived from the profusion of publications associated with the ethylene-platinum system.

The high resolution electron energy loss spectra of Steininger et al. [10] at various temperatures for ethylene adsorbed on platinum (111), reveal three different temperature dependent ethylene species. Below 260K, only the di- σ -bonded species is identified on clean Pt(111) and at high coverages additional vibrations indicate different modifications of the di- σ -species. On a surface precovered with atomic oxygen, some band assignments agree very well with the π -bonded ethylene of the well characterized inorganic complex, Zeise's salt. On the oxygen precovered surface, both π -bonded and di- σ -bonded ethylene coexist. At 250K the adsorbed ethylene decomposes to give hydrogen and water and at higher temperatures carbon dioxide and more water.

On clean Pt(111), Ibach et al. [11] interpreted a new species formed near ambient temperatures to be ethylidene ($=\text{CH}-\text{CH}_3$) formed by a 1-2 hydrogen shift of the di- σ -bonded ethylene. Demuth [12] proposed partial dehydrogenation of one of the carbons on the di- σ -bonded ethylene to result in a vinyl species ($-\text{CH}=\text{CH}_2$). Kesmodel and Gates [13] argued this stable surface species which formed a (2X2) LEED pattern was ethylidyne ($\equiv\text{C}-\text{CH}_3$) formed by a hydrogen shift and a loss of one hydrogen. They used Ibach's HREELS spectra and LEED intensity analysis to derive this structure. The ethylidyne structure seems to presently have

popular support since the careful infrared absorption spectroscopy work by Skinner et al. [14] of an analogous ethylidyne-containing inorganic complex, $(\text{CH}_3\text{C})\text{Co}_3(\text{CO})_9$. An excellent correlation exists between the IR spectrum of the inorganic complex and the HREEL spectrum of the ethylene-platinum system.

Ethylene adsorbs weakly or not at all on an ethylidyne covered surface [15-16] and ethylidyne slows hydrogen coadsorption [17]. Ethylidyne is very stable and does not decompose until 450K to C-H fragments. Another indication of its stability found using [^{14}C]ethylene experiments shows temperatures higher than 500K are necessary to rehydrogenate and remove it from the surface [18]. Rehydrogenation of ethylidyne is not a first order process and it has an activation energy between 5 and 10 Kcal/mole. Deuterium exchange of the methyl group of ethylidyne is possible above 370K.

Soma's infrared spectroscopy studies [19] of ethylene adsorption on supported platinum-alumina contradicts the low temperature HREELS work of Ibach on platinum single crystal surfaces. Soma identifies the π -bonded species as being predominant at 195K with traces of a different unidentified species (possibly the di- σ -bonded ethylene or ethylidyne) whose bands increase in intensity at temperatures above 230K. The unidentified species is not formed when hydrogen preexists on the surface.

Berlowitz et al. [20] studied ethylene adsorbed on Pt(111) under a variety of conditions of clean, hydrogen-covered and oxygen-covered surfaces. On the clean surface the fraction of adsorbed ethylene decomposed decreases with increasing ethylene coverage, while the fraction desorbed as ethylene increases. Ethane was desorbed concurrently with molecular ethylene desorption at 235K. Carbonaceous residues were left on the surface after all thermal desorption (TDS) experiments with ethylene adsorbed on clean Pt(111). On the hydrogen precovered surface, carbonaceous residues were observed only at low hydrogen precoverages. Hydrogen preadsorption split the ethane desorption into two peaks. An ethane peak at 200K moved to higher temperatures with increasing hydrogen precoverage whereas an ethane desorption peak at 260K showed the opposite trend. The ethylene desorption peak broadened and increased to almost 300K with hydrogen preadsorption but shifted to lower temperatures with increasing hydrogen coverage. Ethylene is believed to be adsorbed more weakly on a hydrogen-adjacent site, leading to the lower temperature desorption of ethylene and ethane (which is formed by hydrogenation of ethylene on this site). The hydrogen desorption peaks originating from ethylidyne decomposition decrease in intensity when hydrogen is available on the surface. Hydrogenation appears to be more favored than decomposition with predosed hydrogen under these conditions.

In the TDS investigations [18, 20] the adsorbed ethylene derived species decomposes above 440K on platinum. This TDS peak is very sharp and does not shift with increasing ethylene coverage suggesting a reaction limited peak in contrast to the hydrogen desorption second-order peak which shifts to lower temperatures with increasing hydrogen coverages. This TDS peak corresponds to the loss of two hydrogens from ethylidyne. The hydrogen evolved by the decomposition of ethylidyne immediately recombines in a fast step and desorbs. The decomposition fragments are of two types [17]. The partially hydrogenated carbonaceous fragments are either active or inactive with respect to removal by hydrogenation. The active form undergoes hydrogenation and hydrogen transfer under mild conditions. The inactive residue displays very little reactivity over the entire range of temperatures (300-700K) and pressures (10^{-10} -1 atm) investigated. The inactive residue concentration increases with temperature. Final dehydrogenation of the carbonaceous residue occurs at higher temperatures and leads to the formation of an inactive graphite layer on the surface.

Van Strien and Nieuwenhuys [21] used a field emission probe-hole microscope to determine the relative activity of various platinum faces toward ethylene adsorption over a wide range of temperatures (90-500K). The (111) closest

packed face was the most stable with respect to C-H and C-C bond breaking whereas the stepped (110) face was one of the more active faces.

Kojima et al. [22] used field emission on a platinum tip with a different orientation and received similar results. Their tip showed surface carbide forming at 830K and aggregating into graphite islands at higher temperatures. The graphite concentrated around the (110) direction and migrated into the bulk at 1300K.

Other Metals

As has been shown, ethylene adsorption on platinum undergoes many transformations as a function of temperature. The adsorption of ethylene is also a function of the metal on which it is adsorbed. Ethylene adsorbs on all the group VIII metals but the characteristics of the adsorbed species have differences and similarities on each of the metals depending strongly on the conditions of adsorption [1,2,5,6,7]. Within this group, on nickel, ruthenium and rhodium (and probably iron and cobalt), ethylene forms multiple bonded complexes more easily. Palladium, platinum and iridium form di-adsorbed complexes utilizing two metal atoms upon adsorption. In Figure 2, Ponec [5] illustrated the variation within this chemical group according to their ethylene adsorption characteristics and hydrogenolysis activity. Besides the difference in ethylene adsorption,

the hydrogenolysis or C-C bond breaking tendency is stronger for the first row elements growing less strong toward platinum. Sinfelt [23] tested the relative rates for hydrogenolysis over a variety of supported metal catalysts at two temperatures.

478K Os >Ru >Ni >Rh >Ir >Re >Co >Fe >Cu >Pt, Pd

523K Ru >Rh >Ir >Co >Ni >Pd >Pt

The relative change in rate for nickel is due to self-poisoning of the catalyst by strongly bound carbonaceous species. The hydrogenolysis activity is viewed as a direct measure of the metal's ability to break C-C bonds and form smaller hydrocarbon species. Platinum is a poor hydrogenolysis catalyst and tends to favor large active fragments with intact skeletons which can hydrogenate and desorb. Hence platinum's importance in the hydrocarbon based industries is in its ability to catalyze profitable reforming reactions without simultaneously catalyzing the profit robbing carbon-bond breaking reactions.

Rhodium, nickel and iridium are excellent demethylation, hydrogenation and hydrogenolysis catalysts [1]. They favor small fragments or isolated carbon atoms that rehydrogenate rapidly at high hydrogen pressure. On the (111) face of nickel and iridium, poorly ordered LEED structures from adsorbed small alkenes are found unlike the sharp ordered structures from the same molecules on Pt(111)

[2]. These molecules probably do not have a high mobility on nickel and iridium as they apparently have on platinum. The olefin-metal interaction on iridium and nickel tends to be quite strong reducing the mobility of the adsorbed olefins. TDS spectra indicates the lack of reversible adsorption on iridium and nickel again indicating a strong olefin-metal interaction.

Nickel

A closer look at ethylene-nickel adsorption reveals another complicated adsorption system very different from the platinum case. At low temperatures, on the Ni(111) face a diffuse half-order ring appears in the LEED pattern upon ethylene adsorption whereas on Pt(111) a (2x2) pattern exists [2]. On Ni(001) the diffuse pattern of ethylene adsorption became sharp only upon complete dehydrogenation to surface carbide [13]. HREELS shows two well separated C-H stretching modes from ethylene adsorption on Ni(111) at low temperature [24]. Demuth et al. suggested two of the hydrogens were closer to the surface than the other two. This arrangement would facilitate C-H bond breaking which is evident by the low temperature, 230K, at which adsorbed ethylene loses two hydrogen atoms.

Modulated molecular beam and AES studies [2] have shown the presence of a mobile surface species, with an estimated surface lifetime of 10^{-10} second and a heat of adsorption of

50 Kilojoules mole⁻¹, on an adsorbate-covered Ni(110). The second layer ethylene was concluded when the uptake of ethylene was greater than predicted by Langmuirian kinetics. This loosely bound second layer ethylene species could play an important role in explaining reaction kinetics since its concentration would be sufficient at reaction pressures and temperatures to account for the observed reaction rates.

Iridium

Several of the group VIII metals have patterns for ethylene adsorption similar to that for platinum. The di- σ -bonded species has been identified on rhodium, palladium and ruthenium at low temperatures and ethylidyne has been characterized on the surface of these metals at room temperature. The ethylidyne layer on rhodium [25] and palladium [4] decomposes at around 400K similar to platinum. On ruthenium [26], decomposition was observed starting at 330K possibly due to the stronger metal-hydrogen and metal-carbon bonds which makes the decomposition of ethylidyne via M-H and M-C bond formation more favorable both thermodynamically and kinetically.

Iridium is not mentioned in the above list because ethylidyne was not established on this metal until recently. The TDS spectra from ethylene adsorption on Ir(111) resembles the ethylidyne TDS spectra from the metals for which ethylidyne has been well characterized [27,28]. With

iridium [28], a small amount of molecular ethylene has been observed desorbing with the hydrogen desorption peak normally associated with ethylidyne decomposition.

Arthur and Hansen [29] used field emission microscopy and work function measurements to characterize ethylene adsorption on iridium tips. Emission patterns and work function changes are characteristic of strongly emitting portions (high index faces) and most of the information from these experiments deal with these faces. Above 450K, acetylene and ethylene adsorption were very similar. Above 700K carbonization was evident by intensification of the emission pattern around the (111) planes.

Witt and Nieuwenhuys [30] continued this study using a field emission microscope equipped with a probe-hole assembly to enable studies on individual single crystal surfaces. Stepped faces and the lower symmetry faces have the higher activity and the closest packed high symmetry faces have the least activity. An increase in emission between 260K and the maximum temperature studied (700K) is attributed to C-H bond breaking in the adsorption complex. Additional ethylene can be adsorbed at 90K on iridium previously heated to 400K after exposure to ethylene. Ethylene adsorbed in this state is loosely held and reversibly bound to the surface.

The loosely held ethylene was observed in similar experiments with platinum. An initial reversible emission decrease observed with platinum is missing in the iridium study. The emission increase attributed to a reaction in the adlayer starts at a lower temperature for iridium than platinum for the same surfaces. Iridium surfaces are more active in bond breaking (C-H and C-C) than the corresponding platinum surfaces.

Niemantsverdriet and Van Langeveld [31] using SIMS and Auger electron spectroscopy found at high temperatures, graphitization of adsorbed ethylene is less pronounced on iridium than platinum. The iridium graphitic layer is more amorphous and has a larger hydrogen content at 775K than platinum. Even at 525K graphite formation occurs on platinum whereas on iridium it is much less.

Marinova and Kostov [32] have recently studied ethylene and acetylene adsorption on iridium (111). A saturation coverage of one carbon per iridium atom for both adsorbates was found in agreement with studies on platinum [15]. Another similarity between this work and similar work with platinum is the lack of molecular ethylene thermal desorption. Their HREELS data reveal ethylidyne on iridium at 180K. This is the lowest temperature for which the ethylidyne formation has been observed which agrees with iridium's tendency to break carbon hydrogen bonds being more

pronounced than platinum, palladium and rhodium. At room temperature ethylidyne was found to be partly decomposed. By 500K ethylidyne has completely decomposed and polymerization of the surface carbon is probable. They suggest ethylidyne decomposes to a CCH species.

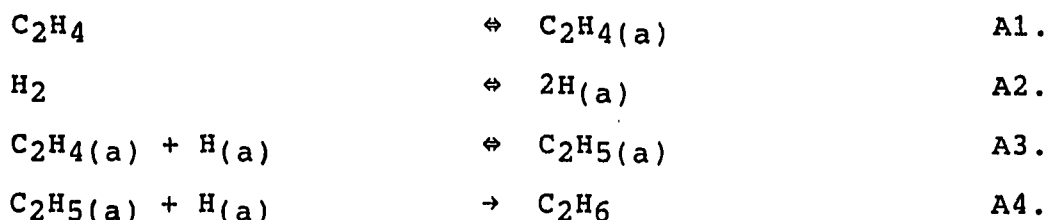
Hydrogen preadsorption before exposure to acetylene on iridium (111) at 300K yields an ethylidyne covered surface similar to ethylene adsorption. If hydrogen is dosed on an acetylene precovered surface, no change in the surface species is observed suggesting the presence of hydrogen adatoms is a necessary condition for hydrogenation.

Kinetics

The complex adsorption characteristics of ethylene on the group VIII metals provide good reasons why the exact mechanism of ethylene hydrogenation has not been resolved. Ethylene hydrogenation is one of the oldest and most studied of all catalytic reactions and unfortunately has remained an unsolved problem in catalysis. Many mechanisms have been proposed but none has been capable of explaining all observations associated with this reaction.

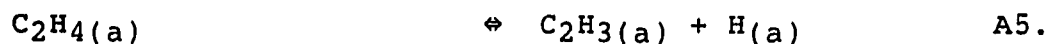
The deuterium distribution in a mixture of hydrogen and deuterium does not depend on whether the mixture is equilibrated or not indicating direct addition of hydrogen molecules does not occur, instead a sequential addition of atomic hydrogen is more probable.

The simplest mechanism and one that still receives much attention is termed the associative mechanism. Horiuti and Polanyi [33] proposed this route in 1934.



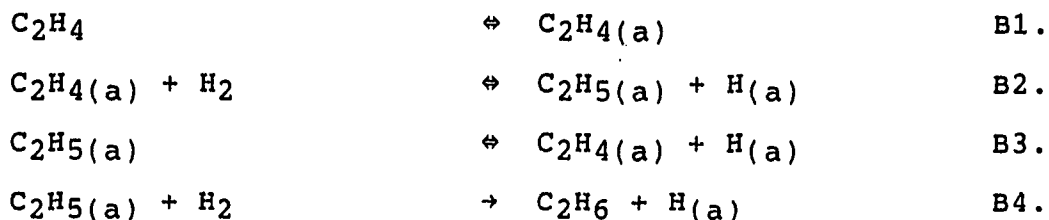
$\text{C}_2\text{H}_4(\text{a})$ represents associatively adsorbed ethylene with the π -bond broken and two carbon-metal bonds formed, the σ -bonded species. Deuterium exchange with ethylene can be explained by the equilibrium of step (A3), the formation of a 'half-hydrogenated state', ethyl species. If step (A4) is the rate limiting step then deuterium distribution in ethane will be random.

Farkas and Farkas in 1938 [34], added an additional step to explain the exchange reaction peaking at high or low amounts of deuterium.

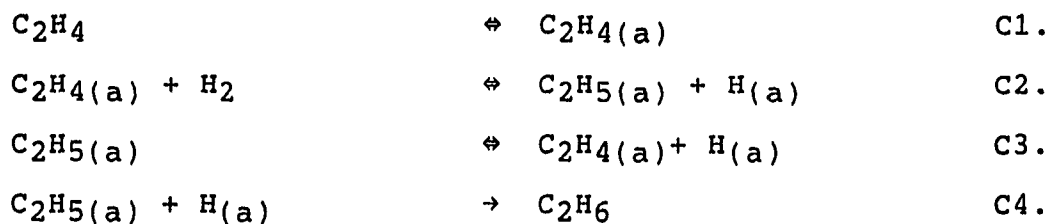


Step (A5) is justified as a separate route because they observed the activation energy for exchange to be greater than the heat of hydrogenation. This mechanism is dubbed the dissociative mechanism because it assumed dissociative adsorption of hydrogen and adsorption of ethylene with rupture of one carbon-hydrogen bond.

Twigg and Rideal [35] in the next year proposed reaction of the adsorbed ethylene with gas phase hydrogen to form the ethyl species and a hydrogen adsorbate or more slowly ethane.

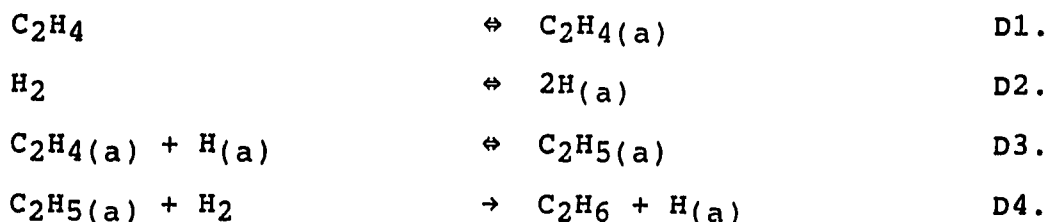


Jenkins and Rideal further modified this mechanism [36].

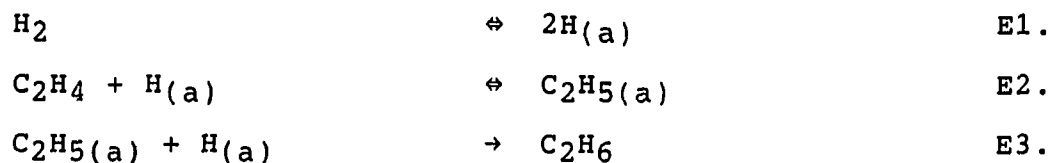


Kinetically it is difficult to discern gas phase and weakly adsorbed molecular hydrogen, so in the above mechanism H_2 can stand for either one. The slow step is assumed to be the interaction between the ethyl-group and adsorbed atomic hydrogen. Assuming hydrocarbon adsorption is fast saturating the surface with adsorbed ethylene, the rate equation is, $rate = kP(\text{hydrogen})$.

Wagner and Hauffe [37] offered another variation of this scheme with adsorbed ethylene and adsorbed atomic hydrogen producing the ethyl adspecies which reacts with gas phase hydrogen releasing ethane and another adsorbed hydrogen atom.



Since the interaction of gas phase hydrogen with adsorbed ethylene was proposed, an obvious alternative is the reaction of gas phase ethylene with adsorbed hydrogen atoms. The relative rates of adsorption of the two reactants led Jenkins and Rideal [36] to assume the surface to be covered with hydrogen atoms and the slow step to be their interaction with gas phase ethylene.

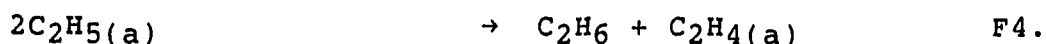
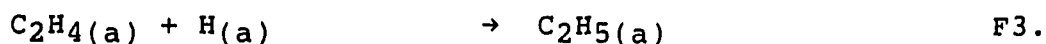
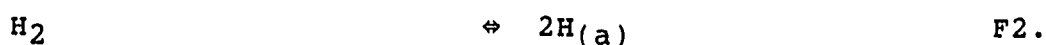
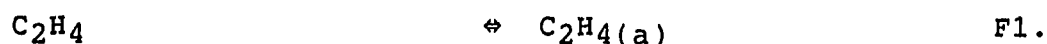


Just as adsorbed ethylene aids in the adsorption of hydrogen in Twigg and Rideal's mechanism, Taylor and Thon [38] proposed hydrogen adatoms to be the sites for ethylene adsorption. A zero order dependence of ethylene is believed by the authors to follow from their mechanism.

The ethyl surface species, an intermediate in many of the mechanisms, has been identified on nickel, cobalt and palladium by the methyl stretching frequency in infrared spectroscopy [39]. The ethyl surface species is also a common intermediate in many of the proposed ethane hydrogenolysis mechanisms. The rate limiting step in this

reaction may be the reaction of a hydrogen adatom with the methyl group on the ethyl surface species and an immediate breaking of the carbon-carbon bond.

Another variation in the ethylene hydrogenation mechanism is the redistribution mechanism [6,40]. Hydrogen is transferred directly from one ethyl group to another ethyl group regenerating an adsorbed ethylene molecule and forming ethane. The ethyl group is formed by addition of a hydrogen adatom to surface ethylene.

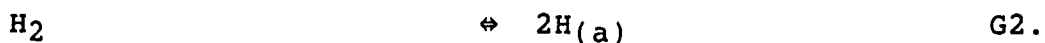


This mechanism was put forward when they failed to observe deuterium initially in ethylene when using it during ethylene hydrogenation.

A common observation is the self-hydrogenation of ethylene to form ethane when ethylene is allowed to react over a metal surface without the presence of hydrogen. Ethane formation under these conditions strongly limits the feasibility of molecular hydrogen interacting directly with adsorbed ethylene. This reaction does suggest the dissociative adsorption of ethylene to release hydrogen atoms which can react with associatively adsorbed ethylene to form ethane.

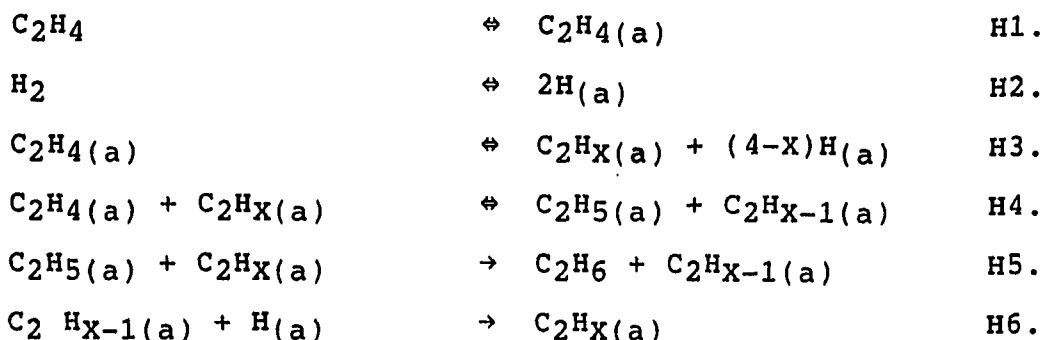
The rate of ethylene hydrogenation is lowered on a surface pretreated with ethylene whereas hydrogen pretreatment does not affect the rate. In the discussion of ethylene adsorption, the dehydrogenated ethylene adspecies were reviewed. The exact role these species perform is not clear. The self-hydrogenation and ethylene pretreatment experiments support their existence and can support their role as a poison.

Gardner and Hansen [41] included the dehydrogenated species in their mechanism but not as a poison. Gas phase ethylene directly abstracts two hydrogen atoms from an adsorbed ethylene molecule to form ethane and an acetylenic adsorbate. The acetylenic adsorbate can be rehydrogenated to enable further reaction.



Ethylene hydrogenation exhibits very little dependence on the nature of the metal catalyst. The dependence of activation energy for different metals varies little as compared to other catalytic reactions. The reaction is not very sensitive to the form the catalyst is in and the reaction is structure insensitive. To explain these and other observations, Thomson and Webb [42] proposed a general

mechanism where hydrogen is transferred between an adsorbed ethylene molecule and a dehydrogenated ethylene species.



Reid et al. [43] had previously studied the retention of [^{14}C] labeled ethylene on many different metals. When [^{14}C] ethylene was preadsorbed on the catalyst surface before hydrogenation with normal ethylene was performed, the amount of [^{14}C] on the surface after and before the hydrogenation was unchanged. The preadsorbed labeled ethylene was inactive to molecular exchange, hydrogenation or evacuation. The persistence of an adsorbed ethylene-derived species on the metal surface during catalytic ethylene hydrogenation ruled out the simpler redistribution mechanism where a single ethylene species acts as both hydrogen donor and acceptor. They did not attempt to propose a structure for the partially dehydrogenated species, only that the carbon-carbon bond is retained. The metal catalyst in this mechanism is sufficiently buffered from the hydrogenation as to reduce its effects on the activation energy as has been observed.

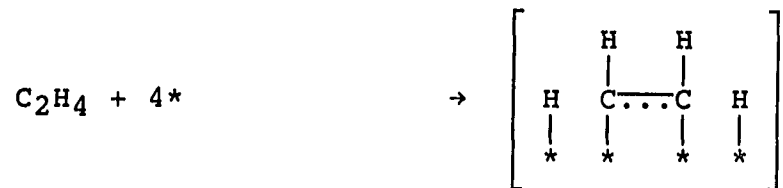
Other workers have identified ethylene in a second layer on top of another more stable ethylene derived adsorbed layer. Weinberg et al. [44] using LEED, flash desorption, atomic and molecular beam scattering and vacuum ultra-gravimetry have identified an irreversible dissociative adsorption of ethylene on platinum (111). On top of this layer ethylene can physisorb in registry with the first layer. They found the second layer to be active for hydrogenation and exchange. A suggested mechanism for hydrogenation involves the second layer ethylene taking two hydrogens from the first layer effectively poisoning that 'site' for further hydrogenation reactions. In the presence of hydrogen gas the poisoned site can be regenerated.

Adsorption isotherms [45] reveal the adsorption of ethylene occurs in two parts over a variety of metals, palladium, rhodium and iridium. A primary nonlinear region in which ethylene is adsorbed directly to the metal surface is followed by a secondary linear region in which it is adsorbed on the first hydrocarbon layer. The primary adsorption is much faster than the second layer adsorption. Hydrogenation is associated with the second layer and occurs in the same fashion as Weinberg proposed.

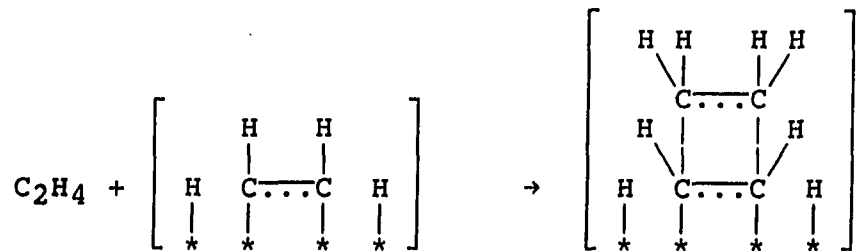
Dus [46] using the static capacitor technique on nickel, palladium and platinum films gave the two layers of ethylene names. He referred to the first layer as the σ -

layer and found it is adsorption with partial dehydrogenation. The second or top layer, he called the η -layer and he found it to contain molecular adsorption. Only the η -layer underwent self-hydrogenation and hydrogenation to ethane at 195K. He proposed the following mechanism.

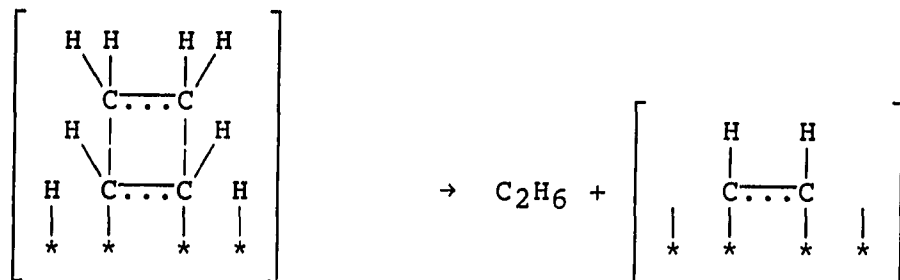
(I1.) Ethylene adsorption in the first layer.



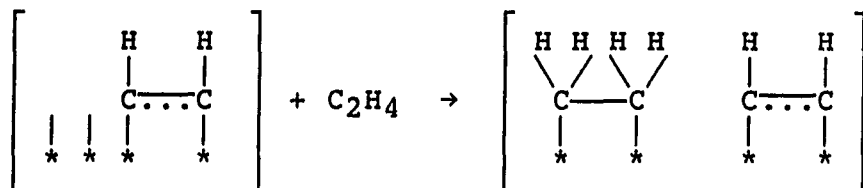
(I2.) Ethylene adsorption in the second layer.



(I3.) Self hydrogenation and ethane desorption.



(I4.) Adsorption of ethylene in the first layer on the sites released in step (3).



or adsorption of hydrogen and repeat of step 3.

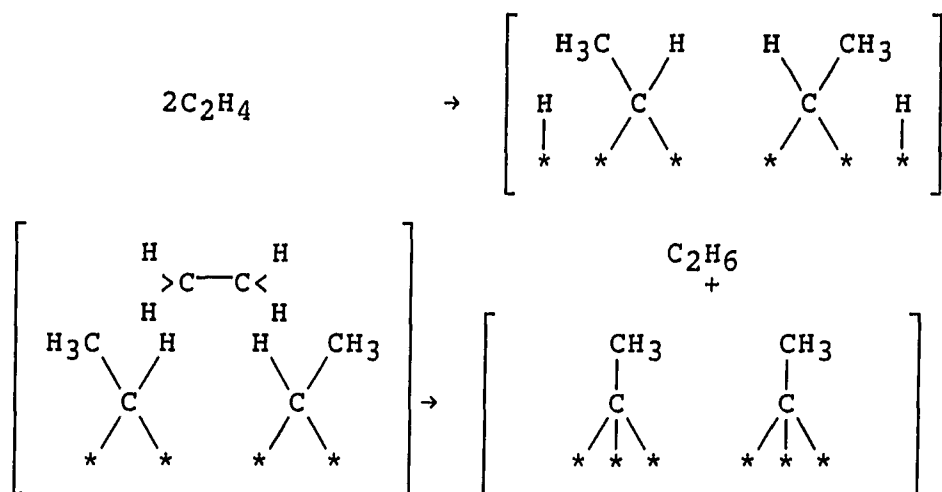
Witt and Nieuwenhuy's [30] field emission microscopy work indicated additional ethylene can be adsorbed on an iridium surface previously heated to 400K after exposure to ethylene. Ethylene adsorbed in this second layer state is loosely held and reversibly bound to the surface. They found similar results with platinum.

Norval et al. [47] used pulsed injection of labeled ethylene in a hydrogen flow over silica supported iridium. Two types of adsorbed ethylene are determined, a long lived state and a short-lived reversible state. At higher temperature, a rise in the level of residual carbonaceous species retained is followed by a similar rise in the initial retention of ^{14}C -ethylene.

Modulated molecular beam and Auger studies [2] on nickel indicate ethylene still adsorbs on a surface after the surface is completely covered.

Spectroscopic characterization of the second layer adsorbed species has not been obtained due to the relative instability of this state. This state is probably weakly adsorbed as a ' π -bonded' moiety which has a weak cross

section in the infrared. The primary region has been characterized as previously discussed and one identification of this region has suggested a second layer mechanism using the ethylidyne species. The ethylidyne species has been characterized on five metals (platinum, palladium, iridium, ruthenium and rhodium) and on all these metals, ethylidyne is stable up to about 530K. Ethylidyne is stable with respect to hydrogenation at room temperature and could be rehydrogenated at 350K on Pt(111) through a nonfirst order process. Zaera [15] and Zaera and Somorjai [18] identified ethylidyne on Pt(111) after ethylene hydrogenation as determined by the LEED pattern and the TDS spectrum. Their mechanism for ethylene hydrogenation involves ethylidyne in the first layer transforming to ethylidene by accepting a hydrogen and then reverting to ethylidyne by giving up that hydrogen to gas phase ethylene.



Zaera's mechanism motivated infrared spectroscopic studies [48] on ethylene hydrogenation over supported palladium. Beebe et al. found ethylidyne forms near 240K, is stable to 400K, reacts rapidly with hydrogen and undergoes deuterium exchange. Only when the ethylene pressure exceeds the hydrogen pressure is ethylidyne formed. During ethylene hydrogenation over a surface predosed with ^{13}C -ethylidyne, the ethylidyne is removed above a critical pressure. The rate of removal is pressure dependent. They concluded ethylidyne is merely a spectator surface species in ethylene hydrogenation over alumina supported palladium.

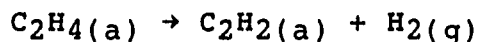
The problem associated with second layer mechanisms is illustrated above. The two layers must be characterized in situ during the reaction. In all second layer mechanisms the second layer is weakly adsorbed and is removed in vacuum. Few studies are done at low enough temperatures to develop a second layer in vacuum. When they are attempted, only liquid ethylene condensed on the surface is evident. No low temperature studies have been attempted on second layer ethylene adsorbed on a stable first layer formed at higher temperatures.

The hydrogen order for ethylene hydrogenation is almost always one for the pressure and temperature range of this study. The ethylene pressure dependence tends to be near zero for most studies. For most of the mechanisms, the partial pressure dependences are easily explained.

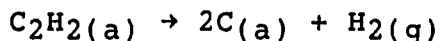
Another common observation which is harder to explain is the optimum temperature for ethylene hydrogenation [32]. The optimum temperature is defined as the temperature at which the rate versus temperature goes through a maximum or local maximum. Seen over a variety of catalysts, it can vary over a broad range of temperature for any one metal. For nickel the optimum temperature has been reported to vary from 308K to 453K. The variation of the optimum temperature is not due to the nature of the metal or to the partial pressures of the reactants.

The obvious way to explain this maximum rate as a function of temperature is to allow a change in the rate determining step at the optimum temperature [32,49]. The temperature dependence of each step in a mechanism is independent of all the other steps in that mechanism such that the relative rates can vary as a function of temperature. Often above the optimum temperature, the addition of hydrogen to the hydrocarbon species to form ethane would be proposed as rate limiting but below the optimum the hydrogen adsorption step is considered rate limiting. The earliest explanation considered olefin desorption as the cause of decreasing rates at higher temperatures. Another explanation proposed by R. Rye [50] assumes the thermal destruction of one of the intermediates in the reaction pathway. He observed two maxima in the

hydrogen thermal desorption from ethylene adsorbed on a tungsten catalyst. The first maximum occurred at 300K which is also the optimum temperature for ethylene hydrogenation over the same tungsten catalyst. He proposed the first hydrogen peak to be from the partial decomposition (or dehydrogenation) of adsorbed ethylene,



and the second peak to be from the complete decomposition to carbon.



Rye attributed the optimum temperature to the decay of the catalyst activity from poisoning by carbon deposition which he assumed to be accelerated above the optimum temperature. Rye extended his theory to include iridium and predicted the optimum temperature to be above 400K because of the absence of any appreciable adsorbed ethylene decomposition below 400K. Nagai and Miyahara [51] found an optimum temperature at 323K over iridium film. Their optimum temperature is too low to fit Rye's prediction. They support the change in rate limiting step theory mentioned above. Their optimum temperature [52] for ethylene hydrogenation over tungsten is 298K in fair agreement with the 300K previously mentioned which would support Rye's theory. Honda et al. [53] did not see an optimum over iridium up to their maximum temperature, 350K.

Obviously ethylene hydrogenation needs further research to clarify its mechanism and to determine the exact role the strongly adsorbed ethylene derived species play. The cause of the optimum temperature is especially intriguing.

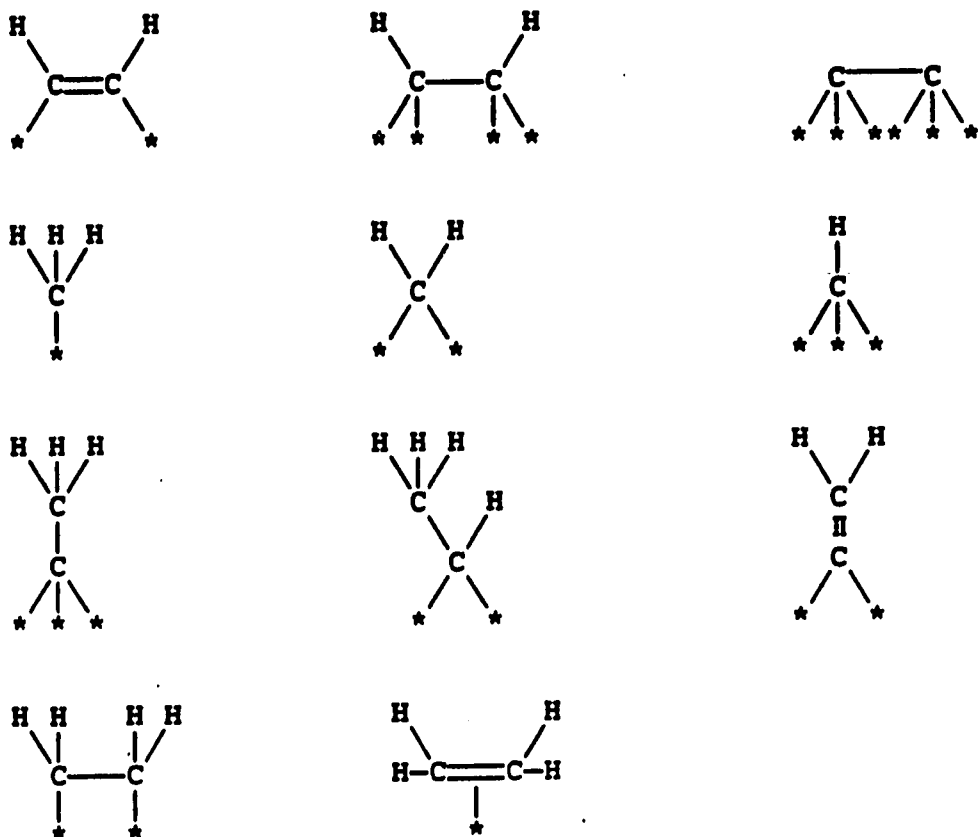



Figure 1. Several forms of ethylene derived surf species

IRON 	COBALT $\alpha \alpha \text{ H}$	NICKEL $\alpha \alpha \text{ H}$
RUTHENIUM $\alpha \alpha \text{ H}$	RHODIUM $\alpha \alpha (\text{H})$	PALLADIUM $\alpha \beta \pi$
OSMIUM $? \text{ H}$	IRIDIUM $\alpha \beta (\text{H})$	PLATINUM $\alpha \beta \pi$

$\alpha \alpha$: high activity in the multiple-bond formation

$\alpha \beta$: an easy formation of di- σ -adsorbed complexes

H : high or medium (H) activity in hydrogenolysis

π : formation of π -complexes

 : carbide formation

Figure 2. Activity pattern of the group VIII transition metals

EXPERIMENTAL

Kinetic Procedures

All kinetic experiments performed for this thesis involved a specially constructed continuously stirred batch reactor interfaced to a UHV chamber as diagrammed in Figure 3. A specially designed sample transfer apparatus enables transfer of the catalyst between the reactor and the analysis chamber. Kinetic analysis is performed by gas chromatographic methods except in the case of isotopic studies where a quadrupole mass spectrometer is used.

A Varian Model 3700 gas chromatograph (GC) is equipped with thermal conductivity and flame ionization detectors for quantitative analysis of the gas phase from the kinetic trials. A self-packed seven foot 0.125" diameter Porapak Q, 80/100 mesh, column is used during most of these studies.

Flame ionization detection (FID) is nearly two orders of magnitude more sensitive for hydrocarbons than thermal conductivity detection (TCD), but fails to detect permanent gases (such as hydrogen, oxygen, carbon dioxide, argon, etc.). The FID quantitative analysis is linear from 0.1 microtorr to 5 torr for the hydrocarbon gases of interest. The TCD and FID detectors are connected in series permitting sequential analysis of the same sample by both detectors.

A Spectra Physics SP4270 Computing Integrator is equipped with a Timed Functions, a Second Channel and a RS-

232C Communications modules. The integrator is programmable in BASIC and contains preprogrammed data acquisition and data reduction routines. Both GC detectors are monitored simultaneously and the reduced data stored for further treatment. The reduced data for all the samples from a kinetic trial are transferred to a laboratory PDP-23 microcomputer for further data reduction. The timed functions module enables control of the GC column oven temperature for precise temperature programming, control of a multiposition sampling valve and a buzzer to inform the analyst when programmed operations are completed.

To increase the accuracy of the kinetic data, a specially designed sixteen-position sampling valve permits sixteen samples to be taken during a kinetic trial in a relatively short time span. No other known study of this type has used such a sampling technique to obtain initial rates. The Valco Model EH ST 16P is equipped with sixteen sample loops with a volume of approximately 1.6 cm³ each. It has been pretensioned for 1000 psi for vacuum work. Gold plated ferrules insure leak-free connections. The integrator is programmable for sequential sampling at precise time intervals via the time functions module and an electric actuator on the multiposition sampling valve. The valve configuration permits trapping of a different time sample in each loop and each sample can be analyzed

sequentially after the last sample is taken. A six port switching valve (Valco Model 6P) fitted for vacuum work connects the sampling valve to the reactor for sample collection or to the GC for analysis.

The sixteen sample loops are calibrated for each product and reactant gas by backfilling all the loops with a mixture where the partial pressure of each component is accurately known and subsequently analyzing the mixtures. Pressures were varied from a few microns to 100 torr for every gas. Figure 4 is an example of the low pressure range calibration graph for ethane. Both detectors were calibrated in the same experiments. The calibration factors for all sixteen loops are depicted in Figure 5 and 6 for the TCD and FID respectively. The sample loops were fabricated from three different stocks of eighth inch diameter tubing resulting in a variation in the loop volume as reflected in the calibration factors.

The conditions of a continuously stirred batch reactor were maintained with a Metal Bellows MB-21 circulation pump in the GC sampling loop. The MB-21 is a virtually leak-free, relatively low pulsating and relatively inexpensive pump. The materials of the pump are high vacuum compatible and very clean. It has the capability to circulate the entire reactor volume at least twice every second through the sampling valve insuring both a truly representative

sample of the reactor at any instant and a well stirred reactor with no concentration gradients.

Another important design aspect is the uniquely small volume of the reactor, 186 milliliters including the entire sampling loop, recirculating pump, valves and environmental chamber. The small volume can be obtained even with a completely evacuated transfer system by the incorporation of a uniquely designed sealing mechanism. A spring-loaded teflon seal isolates the transfer mechanism bellows assembly from the reactor with a sliding compression seal on the sample support tube. The teflon in the seal is reinforced with fiberglass and graphite impregnated for additional lubrication. The teflon seal is a sliding seal allowing transverse passage of a smoothly polished stainless steel tube of uniform diameter. The inner diameter of the seal is a few thousandth of an inch smaller than the outside diameter of the tube creating a compression fit. The seal is captured between a specially machined conflat flange and a custom made replaceable OFHC copper gasket, Figure 7. With a pressure differential of nearly one atmosphere, the pressure in the reactor drops 1-5% during a kinetic trial.

The transfer mechanism shown in Figure 8 used to move the sample from the reactor to the UHV analysis chamber was designed and constructed in Ames Laboratory. The catalyst is spot-welded to two 0.020 inch diameter tantalum wires

which are spot-welded to two 0.032 inch molybdenum conductors on a unique four-conductor minifeedthrough, Ceramaseal or Insulator Seal Incorporated. The other two conductors are chromel-alumel thermocouple feedthroughs for monitoring the catalyst temperature. The minifeedthrough is welded to one end of an approximately twenty-eight inch long smoothly polished one-half inch diameter stainless steel tube. The other end of the tube is welded to a 2 3/4" conflat flange with all the electrical connections running down the tube and out the flange. The tube is housed in a welded bellows assembly allowing 18" of linear movement. The sample tube is supported by a movable carriage on one end and the spring-loaded teflon seal on the other end. The carriage is held by a brass lead screw and two case hardened stainless steel rods via two ball bearing pillow blocks. The front end of the lead screw rides in a brass bushing in a stainless steel front plate. This front plate supports a valved pump-out port, one end of the bellows assembly and one end of the case hardened rods. The back end of the lead screw rides in another brass bushing in another stainless steel plate. This plate supports a worm gear assembly which allows rapid movement through a clutch assembly of the carriage by a reversible variable-speed hand drill or precise positioning with a hand crank. Two dial indicators aid in the accurate positioning of the sample by the

transfer apparatus in the reactor or in front of the Auger optics. Adjustment feet on the front and back plates give vertical angular adjustment for necessary alignment.

The UHV analytical chamber is pumped by two Duniway 20 liter/second ion pumps and an Ultek Boostivac ion pump. The Boostivac incorporates a 25 liter/second ion pump and a titanium sublimation pump in a single unit. One ion pump and the QMS can be isolated by a valve for kinetic studies. A fifty liter/second turbomolecular pump, Balzers TPU 050, is used for initial evacuation of the UHV chamber, during bakeout, and isolated from the QMS during kinetic measurements. Base pressure of the UHV chamber is 3×10^{-10} torr.

The reactor is evacuated by a sorption pump backed by a liquid nitrogen trapped rough pump to ten microns. Higher vacuum conditions, 10^{-7} - 10^{-8} torr, can be reached with another fifty liter/second turbomolecular pump, Leybold Hereaus Turbovac NT50.

Envelope type Bayard Alpert ionization gauges, Granville Phillips Gauge Controllers Series 271, are placed near each turbomolecular pump and ion pump. Fast response thermocouple gauges, Thermionics Model 104, monitor the pressures of each backing pump of the turbomolecular pumps and the sorption pump. A Schulze Phelps ionization gauge, Cooke Vacuum Products, monitors the pressure of the gas

dosing manifold. Two capacitance manometers, MKS Baratron, are used to accurately create the kinetic trial mixtures. The two capacitance manometers span from 10 millitorr to 10,000 torr.

The benefits derived from the adopted set-up over previous designs include the rapidity of sampling. In all other studies each aliquot must be fully analyzed before another sample can be taken. Several minutes will transpire between samples. In kinetic studies of this type, only the steady state rates can be taken. Initial rates instead of steady rates can be determined in the set-up used in this thesis. With initial rates the product concentration is low enough to neglect the influence the product may have on the rate and the buildup of surface contamination is held to a minimum. The reliability of the rates is greatly enhanced by the greater number of measurements taken during a single kinetic trial. Most studies of this type rely on only a few samples per run. With sixteen samples taken during a single trial, the accuracy of rate determination is significantly increased, especially for very fast rates or very slow rates with low concentrations.

Another benefit concerns the dilution effect seen in other studies. When a sample is taken in a conventional set-up, during the injection, GC carrier gas is introduced into the reactor stream. The carrier gas acts as a diluent

in the next sample. The dilution effect is avoided in this set-up by backfilling every sample loop with the reactant mixture before a kinetic trial is begun. During sampling this initial concentration is replaced with a timed sample of the reaction feed. For initial rates where less than 10% of the reaction has proceeded, the repeated injection of the initial mixture into the reactor has a negligible effect on the concentrations.

Crystal Preparation

All the iridium single crystals used in this study were cut from the same boule. Small bubbles in the the boule contributed less than 0.1% polycrystalline surface area to the total surface area of the aligned single crystal slices. All the (111) aligned crystals were prepared by me. I cut, aligned both sides and polished several (111) crystal slices for use in this thesis.

A homemade Bond type adjustable barrel holder goniometer [54-56] was used in realigning or aligning single crystal disks to within a half-degree of orientation. The crystal slice is cemented with a generous portion of thermoplastic to an aluminum piston which fits in a cylinder. The piston gains movement in the cylinder by a spring tensioned adjustable screw. The cylinder is held inside an aluminum housing by two sets (front and back) of three adjustment screws. The two sets of screws are

tightened against flats on the cylinder preventing the cylinder from rotating and allowing angular adjustment of approximately seven degrees. The angular positioning was attained by loosening one/two screw(s) and tightening the other two/one screw(s). The goniometer was tested for trueness using a low power He-Ne laser and a V-block. The laser beam was reflected from the highly polished steel front rim of the goniometer onto a wall 13 feet away. The goniometer was rotated in the V-block and the movement of the reflected beam carefully monitored. Very little movement of the beam was observed indicating the face was perpendicular to the sides of the goniometer to within a few minutes. The beam was then reflected from the crystal face mounted on the goniometer and the process repeated. The angular position of the crystal was adjusted to give no movement of the reflected spot. The crystal face was now in the same plane as the front rim of the goniometer and perpendicular to the axis of rotation. Laue x-ray diffraction pictures of the crystal slice in several rotational positions were taken using the same V-block. This procedure accurately determined if the physical surface and crystalline face were identical. This procedure was used several times during the alignment process to verify the alignment. A different Bond barrel holder was used on one of the crystals with similar results.

The homemade goniometer was used to grind the crystals to alignment. The crystal was mounted as previously discussed. Using the angular adjustment screws the crystals were oriented to put the $\langle 111 \rangle$ direction in line with the rotation axis of the goniometer. This is determined by Laue backscattering x-ray diffraction. The Laue pattern for the (111) face is centered on the film by making all the diffracted spots symmetric about the primary x-ray beam spot. The translational position of the crystal was adjusted to place the crystal just outside the plane of the goniometer face. The crystal is ground with 240, 360, 400 and 600 grit abrasive cloths on a grinding table. The crystal is rotated 90° between each of the grits making it easier to see when the damage from the previous grit is removed and to minimize the amount of deep structural damage to the crystal. The grinding movement was always in the same direction for each of the grits. Rough polishing of the crystal was done with a polishing wheel covered with billiard cloth and soaked with an alumina slurry. The crystal was accurately mounted in Acrylic plastic and finally polished on a vibrating polishing wheel. Linde A (0.5 microns) was used for five hours and Linde B (0.03 microns) was used for a minimum of two hours. The final alignment was checked to be within half-degree for all crystals used in this thesis.

Catalyst surface areas were calculated geometrically for the faces and edges. Total areas of the crystals were approximately one square centimeter each with the aligned surface area exceeding 85% of the total area. A conversion factor of 1.566×10^{15} atoms/cm² was used to determine the number of metal sites on the (111) surface (normally between 1.67×10^{15} to 1.58×10^{15} metal sites per crystal).

Sample Cleaning Procedure

Chemical and high temperature cycling techniques were used to insure the entire catalyst surface reached the same degree of cleanliness. Only one face of the catalyst was subjected to Auger analysis for determination of the impurity levels whereas the entire catalyst surface contributed to the kinetics and TDS results. A combination of heating between 600K to 1000K in a gaseous environment (oxygen to remove carbon and sulfur, hydrogen to remove oxygen) and flashing to 1200K-1400K left a surface virtually free of any contaminants. After ethylene hydrogenation, heating in oxygen at 673K followed by flashing to 1300K would return a surface free of contaminants with the exception of a small quantity of oxygen. The residual oxygen coverage was estimated by AES to be less than a quarter monolayer in all cases and less than a tenth monolayer in most hydrogenation trials.

Auger Electron Spectroscopy

Auger electron spectroscopy (AES) was used throughout this study to monitor the elemental composition of the iridium surface. AES was conducted using a retarding field electron energy analyzer (PHI four grid electron LEED optics, Model 10-180). Auger analysis gave an elemental analysis of the surface region before and after the kinetic experiments. The results were semiquantitative and did not give any information on the chemical environment of the surface; only the elemental composition could be determined. Auger analysis verified that all the contaminants on the surface were removed prior to a catalytic reaction. After a kinetic trial was completed, the ratios of the carbon and iridium peak-to-peak heights were recorded for comparison under varying conditions.

The Auger effect involves emission of electrons from a substance by an autoionization process that arises from the electrostatic interaction between two electrons in an atom after the initial creation of a core hole. In this thesis the initial hole is created by the scattering of very energetic electrons (1-1.6 keV) by the surface. An outer shell electron will relax to the inner shell vacancy, releasing energy which is transferred to a second electron which is subsequently ejected. The ejected or Auger electron has a characteristic energy

$$E_{ijk}(z) = E_i(z) - E_j(z) - E_k(z-\Delta) - e \cdot \phi_{sp}$$

where the subscripts i , j and k represent the electronic energy levels involved in the process, z is the atomic number of the atom, Δ is the effective charge after the initial ionization, and ϕ_{sp} is the work function of the spectrometer referred to vacuum. $E_k(z-\Delta)$ includes a correction due to electronic relaxation of the environment surrounding the ionized atom. The energy, E_{ijk} , is characteristic of the element from whence the electron originated permitting the determination of elemental compositions. The yield of the ejected Auger electrons is proportional to the elemental composition but absolute quantitative analysis is hindered by the complex process involved in the Auger phenomena, and quantitative results are most reliable when based on calibrations against known coverages (obtained, e.g., from coverages with known structures).

The energy of the Auger electron is a function of three separate energy levels, one of which is not an energy level of the neutral atom but an energy level of the ionized atom. The resultant kinetic energy is very broadly dispersed and is sensitive to the chemical environment in a complex manner. Auger spectra are often, as in this study, taken in the derivative mode to enhance the sensitivity of the analysis. To extract quantitative quantities from the derivative spectrum, the distance from the maximum to the

minimum pen excursion in the Y-direction is measured as the peak-to-peak height. The relative peak-to-peak height ratio of a contaminant peak to an iridium peak is used to judge relative effects and coverage trends. Quantitative accuracy was hindered in this study due to the large level of noise in all the spectra. Retarding field analysers have a poor signal-to-noise characteristic which is complicated by the surface concentrations of interest in this thesis. Exact quantities are not determined in this work but trends in relative surface concentrations are documented.

Figure 9 is a block diagram of the Auger electron spectrometer used in this thesis. The AES system control (PHI Model 11-500A) had been modified by Physical Electronics to be used with a standard LEED set up. A Princeton Electronics Model 128A lock-in amplifier similarly modified was used in the AES detection circuit. A four grid retarding field analyzer (PHI Model 10-180), in which the first and fourth grids are grounded, sorts the electrons by their kinetic energy by imposing a potential barrier of known height between the sample and the collector. Electrons with energy greater than the applied potential can reach the collector and are detected and all other electrons are repelled. This potential is applied to the second and third grids. The collector potential is set to attract and trap the electrons which pass the potential barrier. The

collector potential in this thesis is applied by three 45 volt batteries. A small ac modulation voltage is added to the analyzer potential and measuring the in-phase component of the ac current at the modulating frequency as a function of the applied dc voltage gives an energy spectrum. The Auger peaks are superimposed on a slowly varying large background of secondary electrons. To better detect the Auger peaks, the second derivative of the retarding potential curve is obtained by measuring the second harmonic component of the collector current. The second derivative current versus applied potential curve is plotted on a X-Y recorder.

Thermal Dehydrogenation Spectroscopy

Thermal desorption spectroscopy (TDS), sometimes called thermal programmed desorption (TPD), provides information on adsorption states, populations, energetics of bonding, chemical reactions on surfaces and adsorbate-adsorbate interactions.

In the TDS experiment the solid sample is heated in a linear fashion and the gaseous environment about the sample is monitored with mass spectroscopy. Adsorbed gases are quantitatively detected as they desorb from the surface. In this thesis the adsorbed species decomposes/dehydrogenates to give another surface species and hydrogen gas.



The partial pressure of hydrogen detected in the TDS experiment characterizes the stability of the adsorbed carbon species and measures the degree of hydrogenation of this species. In this thesis TDS can equally mean thermal dehydrogenation spectroscopy.

Experimentally, as shown in Figure 10, the linear temperature ramp was obtained by interfacing a Micro PDP-11 dedicated laboratory computer to a Hewlett Packard 6286A DC Power Supply which supplied the heating current to the sample support wires. The HP power supply was controlled by a DAC output voltage whose output was increased quadratically in x (output = $Ax^2 - Bx + C$) to give a time linear temperature ramp. A , B and C are empirically found parameters and x is a program index number which is increased after every set of measurements. Examination of the quadratic equation reveals an initial higher current pulse due to the value of C which desorbs gases from the support wires previous to the smooth linear ramp. The sample temperature was followed by a chromel-alumel thermocouple spot welded to the back of the sample. The thermocouple was connected to an Omega Digital Temperature Indicator equipped with the analog output option. The analog output gives 1 mV/°C and was interfaced to the Micro PDP-11. The mass spectrometer used in this thesis work, a UTI 100C quadrupole mass spectrometer, was also interfaced

to the Micro PDP-11. Up to five masses could be followed during a single TPD experiment with a reasonable temperature ramp (5-10K/second). Slower ramp times allow the monitoring of more masses but with decreased sensitivity. The elapsed time, temperature and mass spectral intensities for each mass were collected and stored in a file for future data analysis and plotting.

Table 1. List of reagents with sources, purities and major impurities

Reagent	Source	Purity	Impurities
Oxygen	SGP ^a	99.999%	LT ^b 1 ppm N ₂ O, K, Ar, Xe, CO ₂ LT 3 ppm H ₂ O LT 5 ppm N ₂ LT 0.5 ppm CH ₄
Ethane	Matheson	99.99%	LT 6 ppm CO ₂ LT 34 ppm C ₂ H ₄ LT 5 ppm He
Argon	SGP	99.9995%	LT 1 ppm H ₂ O, H ₂ , O ₂ LT 0.5 ppm CO ₂ , CH ₄ LT 3 ppm N ₂
Hydrogen	Liquid Air	99.99%	LT 0.5 ppm THC ^c
Ethylene	SGP	99.98%	
Deuterium	Scott	99.7%	

^aSGP Scientific Gas Products.

^bLT Less Than.

^cTHC Total Hydrocarbon.

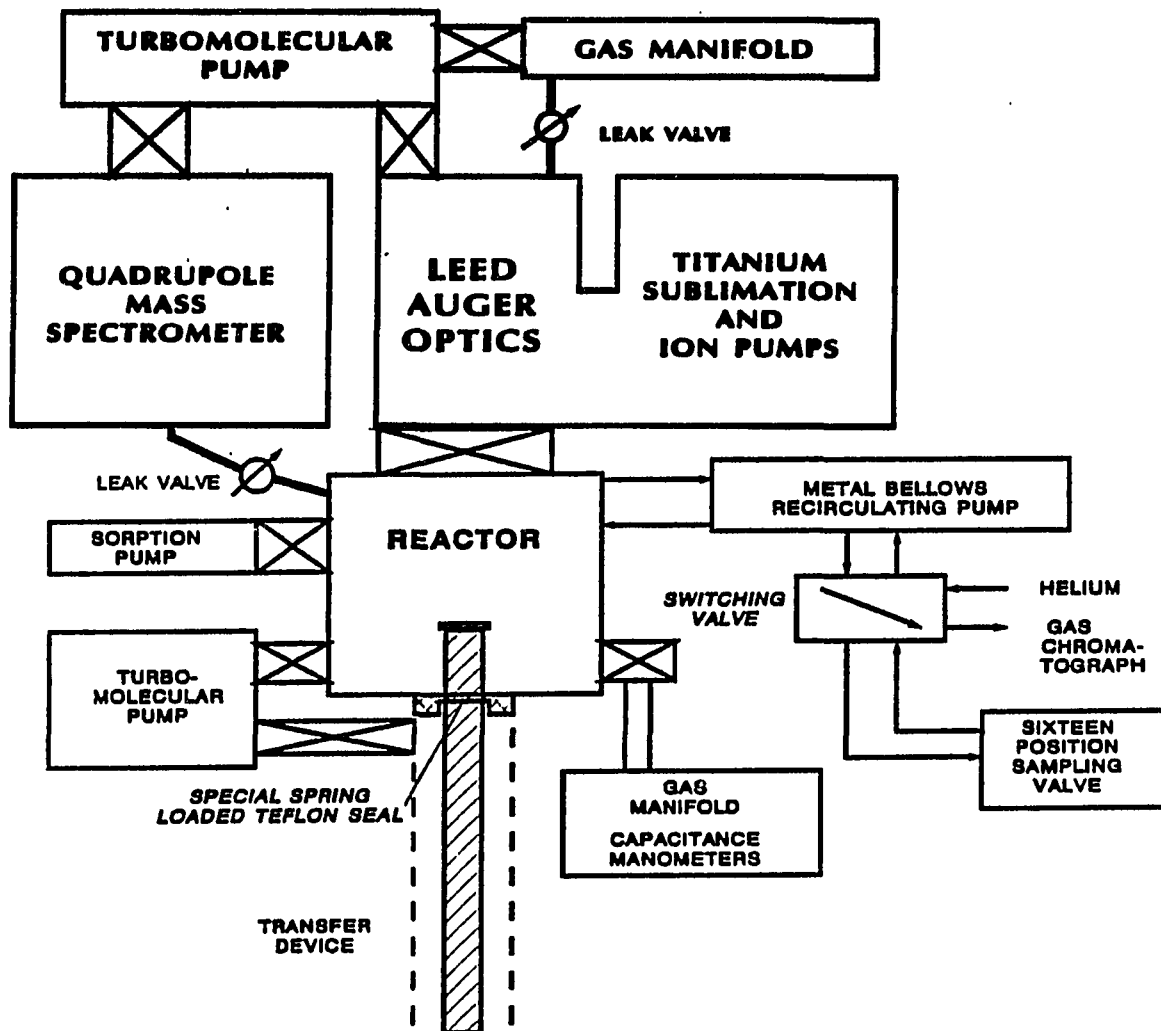


Figure 3. Schematic diagram of catalytic reactor showing the gas sampling loop, gas handling manifold, pumping system and sample transfer apparatus

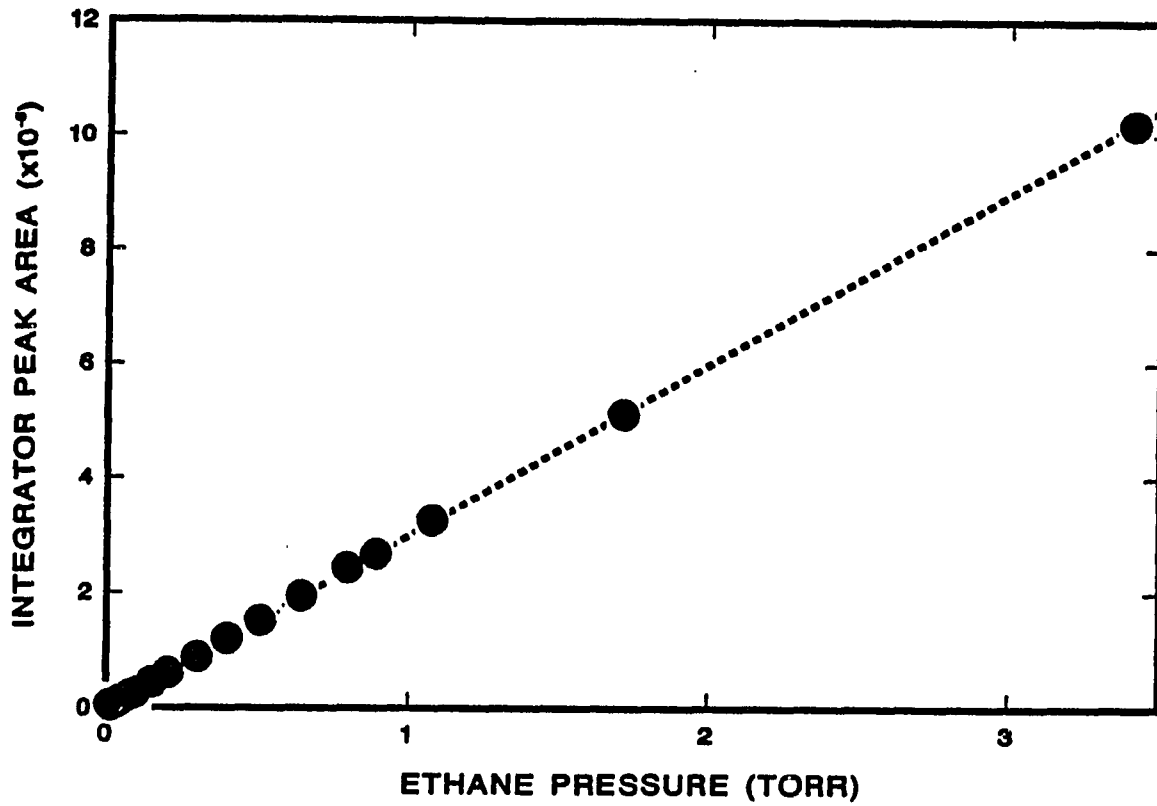


Figure 4. Calibration curve of the flame ionization detector response versus the ethane pressure for the low pressures used in this thesis

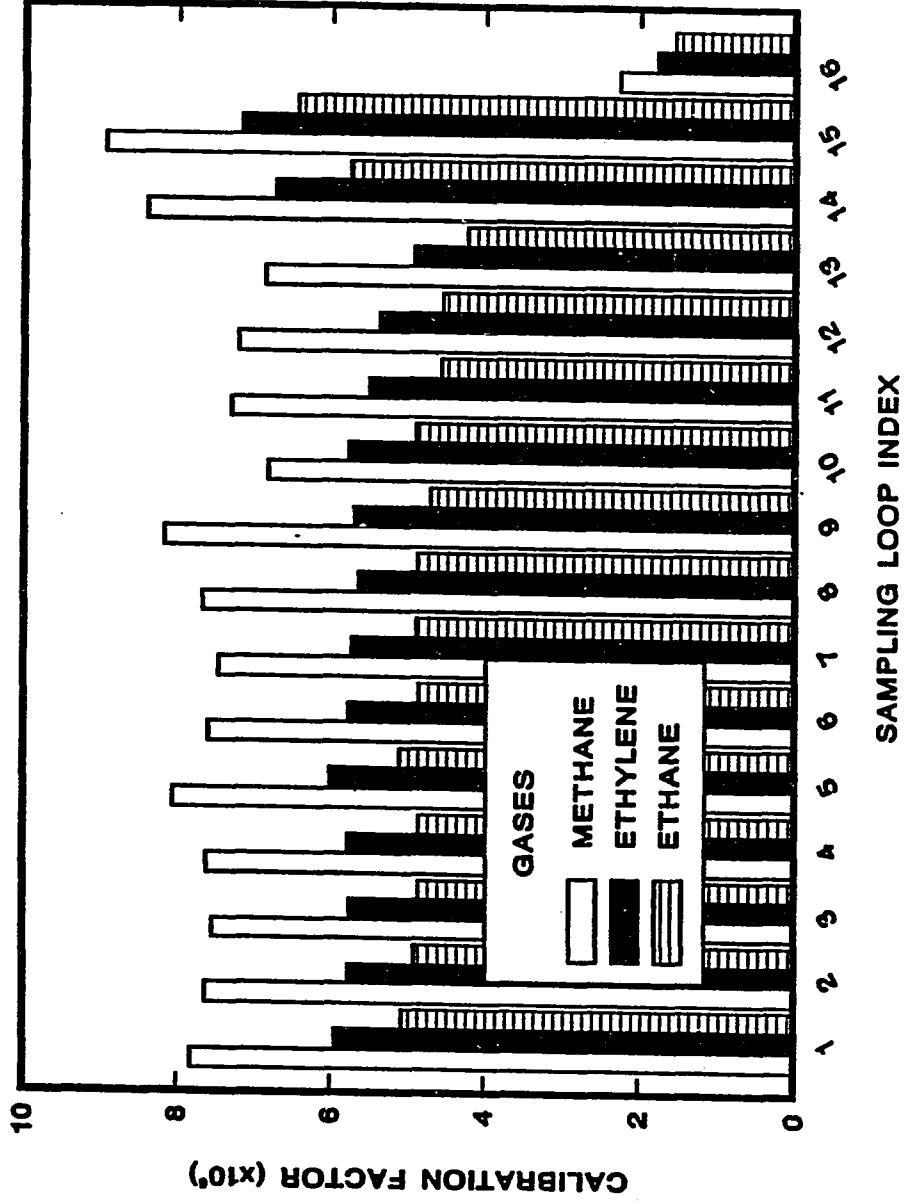


Figure 5. The thermal conductivity detector calibration factors for all sixteen sample loops for the gases considered in this thesis

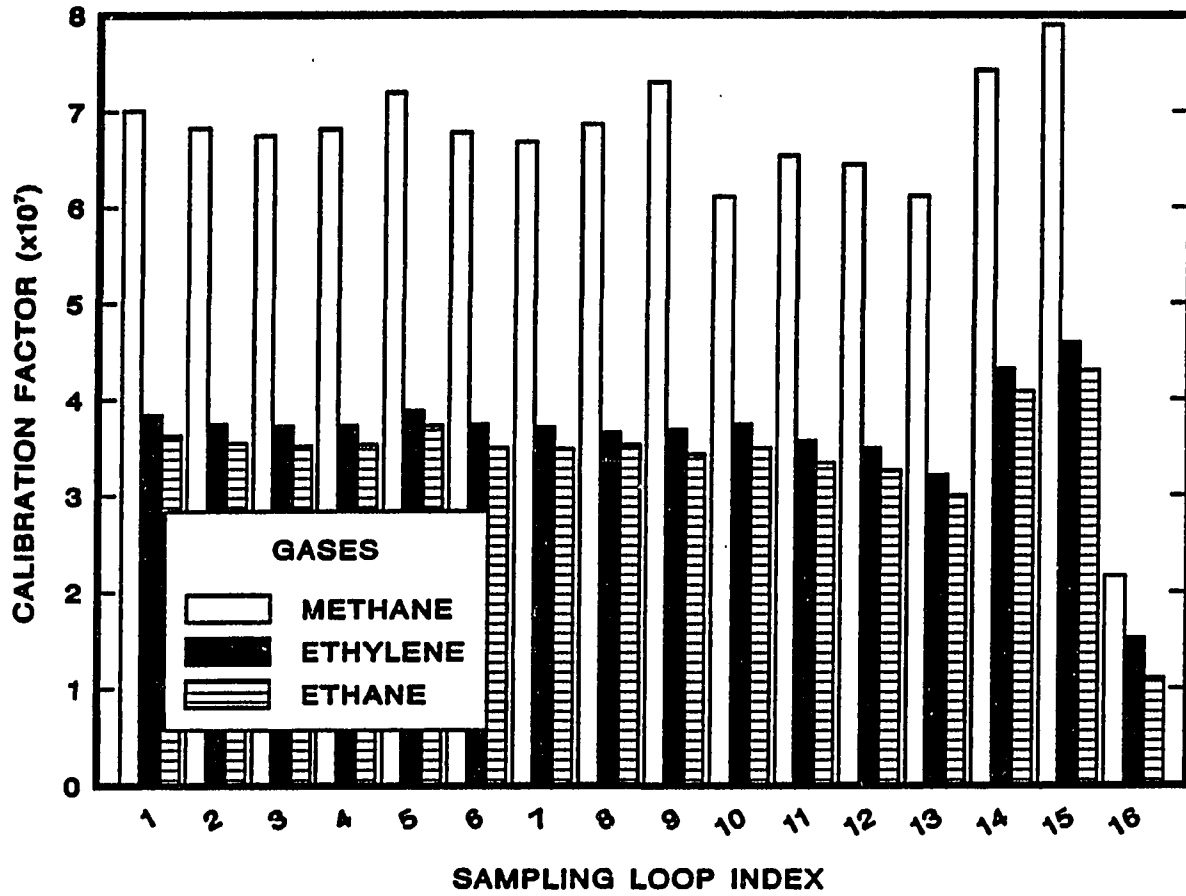


Figure 6. The flame ionization detector calibration factors for all sixteen sample loops for the gases considered in this thesis

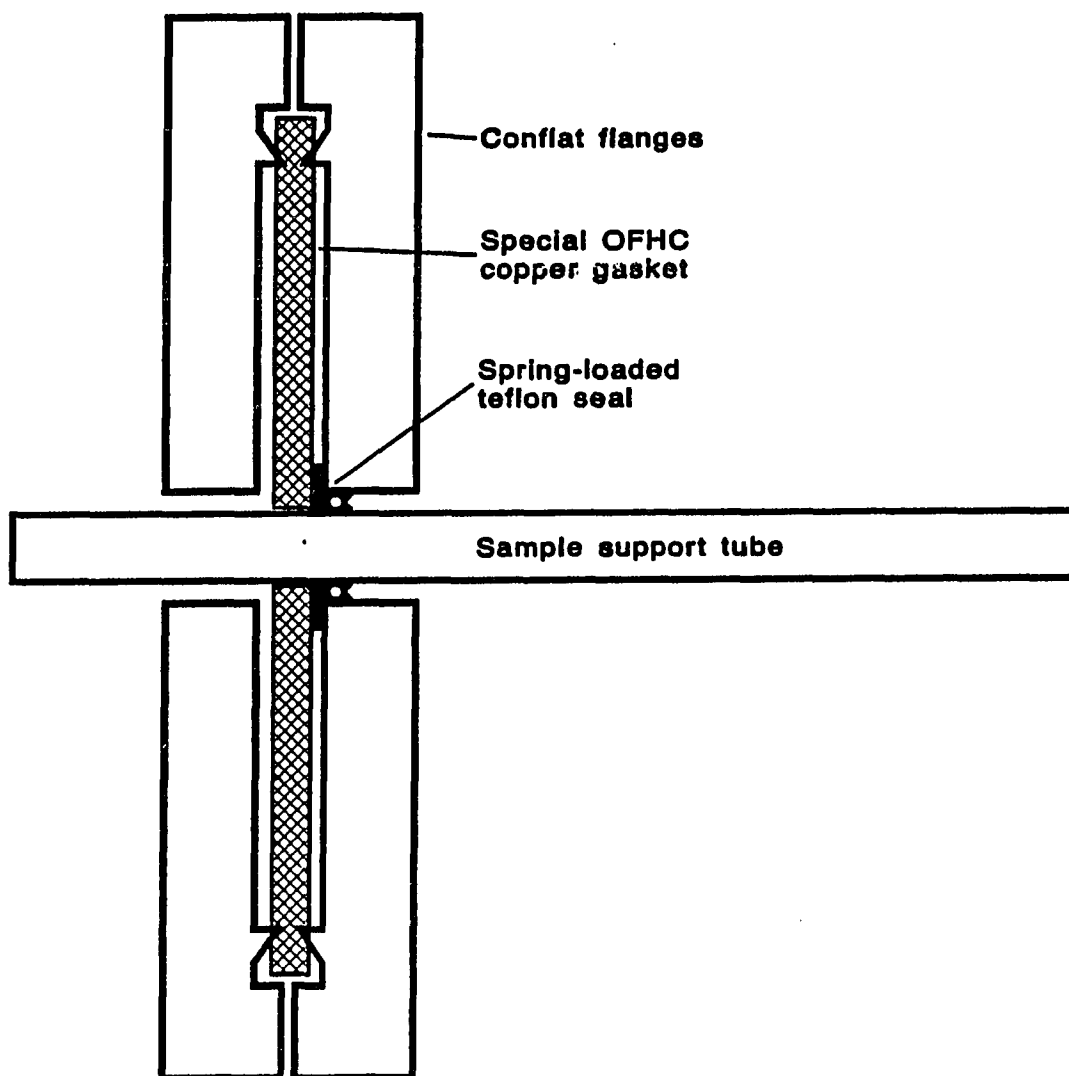


Figure 7. Schematic representation of the spring-loaded teflon seal used in isolating the reactor from the sample transfer apparatus

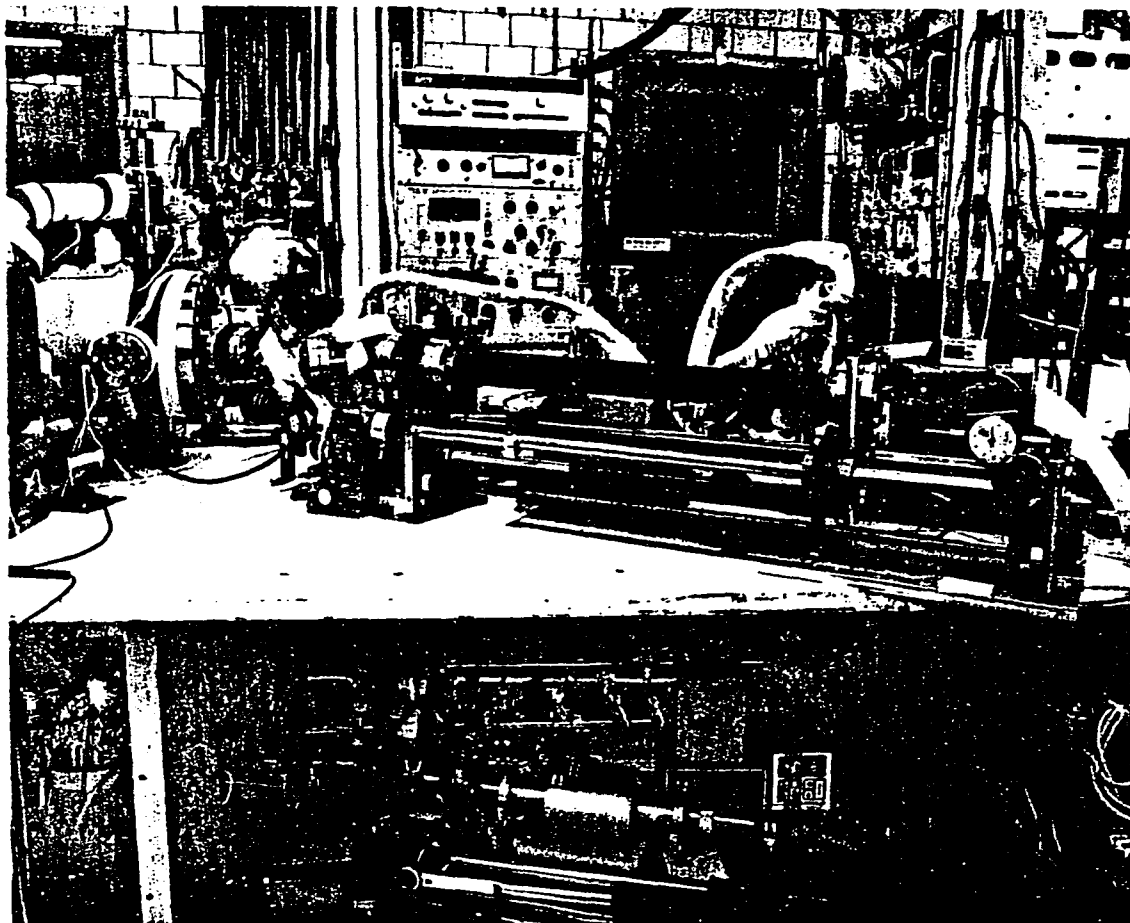


Figure 8. Ames Laboratory fabricated sample transfer apparatus used to move a sample in vacuum from the reactor to the ultra-high vacuum analysis chamber.

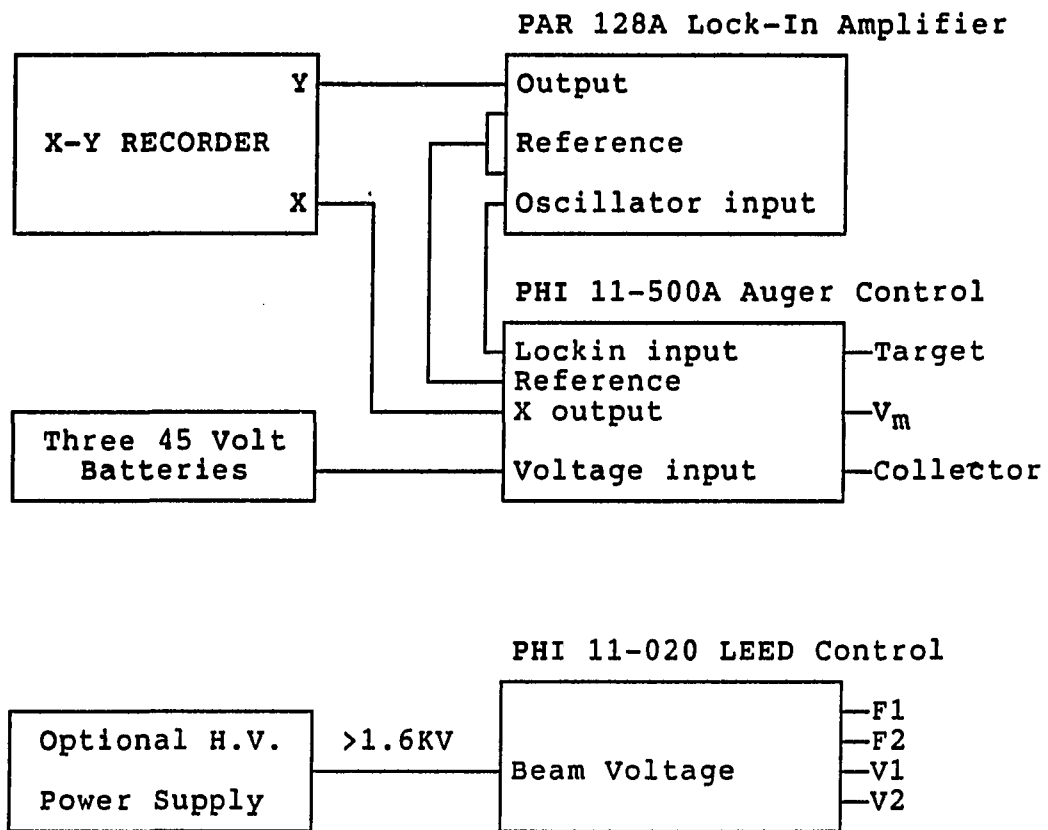


Figure 9. Schematic diagram of the Auger electron spectroscopy electronic components

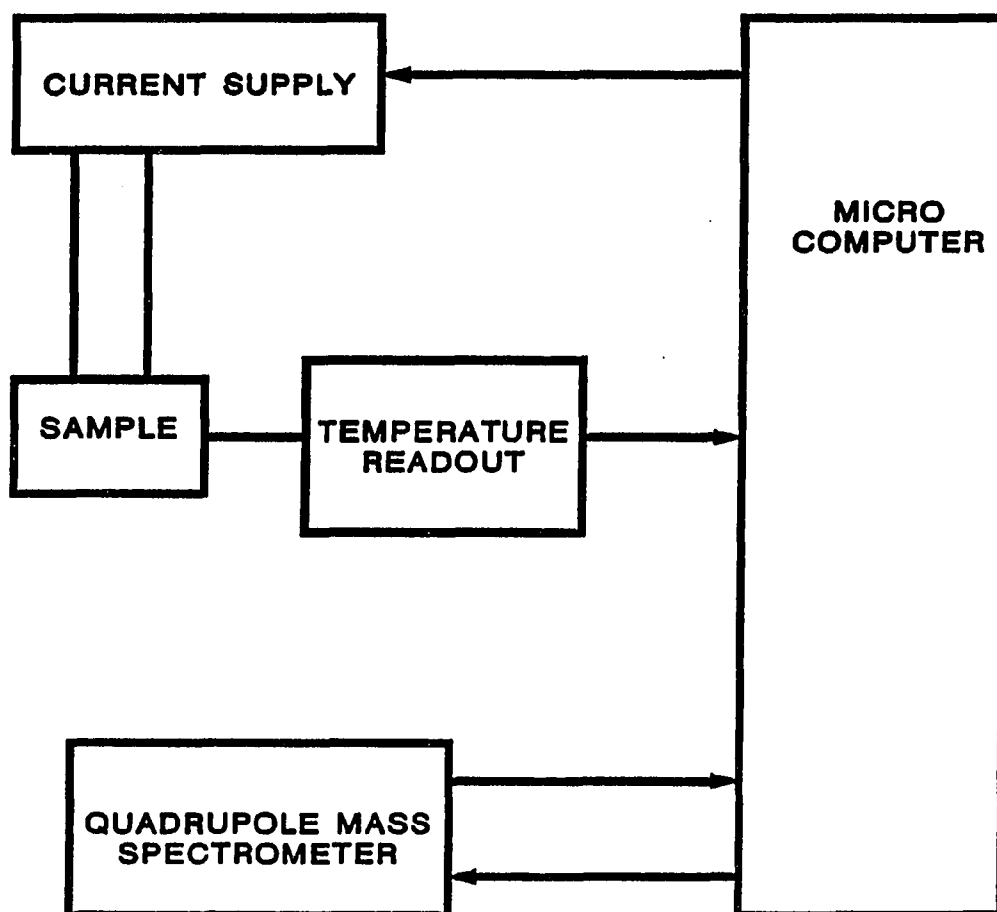


Figure 10. Schematic diagram of the thermal desorption spectroscopy experimental set-up

RESULTS AND DISCUSSION

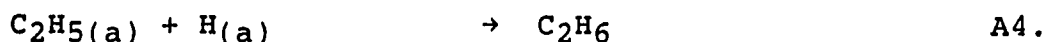
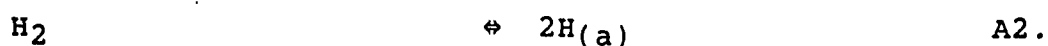
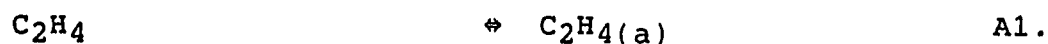
The initial reaction rates were determined using a least squares fit of the product concentration versus time near zero time (Figure 11). For initial rate determinations first-order kinetics are assumed for the reactants. Any further reaction of the gas phase product, ethane, can be neglected due to ethane's low probability of adsorption and extremely low relative concentration near zero reaction time. Turn-over numbers are calculated from the measured rates, the volume of the cell and the number of active sites. The number of active sites is calculated from geometric considerations of both crystal faces and its edge to determine the number of iridium surface atoms.

Hydrogen Dependence

The hydrogen order taken from a plot (Figure 12) of the log of hydrogen pressure versus the log of the turnover number is 0.98 at 473K. Hydrogen partial pressure was varied from 0.4 to 626 torr. The ethylene partial pressure ranged from 0.4 to 0.5 torr and averaged 0.44 torr. Reviews generally quote a value of one for the hydrogen order in the pressure and temperature range studied. Hydrogen dependency runs made without Auger analysis to determine the surface integrity before hydrogenation show more scatter in the rate measurements than the runs made with a well characterized surface. A run with a surface contaminated by carbon

according to Auger analysis revealed a lower rate than the clean surface. Therefore, runs where surface cleanliness had not been established by AES were discarded even though a general cleaning procedure had been performed just prior to the run. If these runs were included in the order plot, they would not have significantly changed the final order value but would have increased the scatter in the plot.

A hydrogen order of one follows if one assumes a modified Horiuti and Polanyi [33] mechanism (mechanism A in the literature review section) and a rate limiting surface reaction step of an adsorbed hydrogen and a partially hydrogenated ethylene adspecies, step A4. The surface is



nearly saturated with ethylene species at the high ethylene pressures used in this study and above the temperature of hydrogen desorption, ~370K, the hydrogen coverage is quite low. Assume at 473K, the hydrogenation rate is controlled by a surface reaction, either steps A3 or A4. If step A3 is chosen, a steady state approximation of the surface concentration of $\text{C}_2\text{H}_5(\text{a})$ gives,

$$\begin{aligned} \text{rate} &= k_3[\text{H}(\text{a})] \\ &= k_4[\text{H}(\text{a})][\text{C}_2\text{H}_5(\text{a})] \end{aligned}$$

Substituting using step A1 and $\theta_{\text{H}} \ll 1$,

$$[H_{(a)}]^2 = K_2 P_{H_2}$$

$$[H_{(a)}] = (K_2 P_{H_2})^{1/2}$$

$$\text{Rate} = k(K_2 P_{H_2})^{1/2}$$

But a hydrogen order of one was experimentally determined, so A4 is considered as the rate limiting step. If step A3 is in equilibrium,

$$\begin{aligned} [C_2H_5(a)] &= K_3 [H_{(a)}] \\ &= K_3 (K_2 P_{H_2})^{1/2} \end{aligned}$$

$$\begin{aligned} \text{Rate} &= kK_4 [H_{(a)}] [C_2H_5(a)] \\ &= kK_4 K_3 K_2^{1/2} P_{H_2} \end{aligned}$$

The hydrogenation rate will be first order in hydrogen with this mechanism.

During all but the lowest hydrogen partial pressure runs, methane production was observed. The hydrogen order for the methane production reaction (Figure 13) is very roughly one but the confidence level of this result is very low. The amount of methane produced is quite small and measurement of the initial rates is correspondingly not very accurate. An obvious increase in initial rate with hydrogen partial pressure is evident. The methane is not from the hydrogenolysis of ethane, the hydrogenation product, but is believed to originate directly from ethylene. The ratio of

the hydrogenolysis rate to the hydrogenation rate (Figure 14) does not increase as would be expected if the two were sequential reactions but the ratio decreases with hydrogen pressure.

Ethylene Dependence

Ethylene partial pressure dependence (Figure 15) at 473K was not as simple as the hydrogen dependence. The ethylene pressure was varied from 0.077 to 588 torr with hydrogen partial pressure held constant at 100 torr. From 0.077 to approximately seven torr, the ethylene order plot was linear with a slope of one but at higher ethylene partial pressures the plot leveled-off.

The behavior of the ethylene order plot is indicative of adsorption of ethylene leading to saturation at higher ethylene partial pressures. The literature rarely reports such a behavior for the ethylene dependence and often gives zero dependence of the rate on ethylene pressure. These investigators work at an ethylene to hydrogen pressure ratio greater than one which gives them zero order at their working temperature. These results do not disagree with this result, instead this result supplements the past results.

Various possible kinetic mechanisms for the ethylene dependence data were tested by rearranging the equations to a linear form for applying a least squares fit of the

experimental data. The least-squares fit determined the parameters of each model. In Langmuir-Hinshelwood kinetics the rate is determined by the concentration of surface species which can be related to the gas phase over the catalyst via isotherms. The Langmuir isotherm relating the surface concentration to the pressure is given as,

$$[H(\text{ads})] = \frac{aP_H}{1 + aP_H}$$

where a is the adsorption-desorption equilibrium constant for species H (hydrogen). For two species reacting on the surface and competing for the same sites, the rate is a product of the isotherms, where b is the adsorption-desorption equilibrium constant for species E (ethylene).

$$\begin{aligned} \text{rate} &= k [H(\text{ads})][E(\text{ads})] \\ &= k \frac{aP_H bP_E}{(1 + aP_H + bP_E)^2} \end{aligned}$$

As previously discussed the hydrogen pressure showed a first order dependence when hydrogen pressure was varied as the ethylene pressure was held constant. In the above equation abP_E and $(1 + bP_E)$ are constants and $aP_H \ll 1$.

$$\begin{aligned} \text{rate} &= \frac{(kaP_E b)P_H}{(1 + bP_E)^2} \\ &= k'P_H \end{aligned}$$

$$\text{with } k' = k \frac{abP_E}{(1 + aP_E)^2}$$

Using the Langmuir-Hinshelwood equation to describe the limiting behavior of the rate dependence on ethylene pressure with $aP_H \ll 1$,

$$\begin{aligned} \text{rate} &= k \frac{aP_H bP_E}{(1 + bP_E)^2} \\ &= k'' \frac{bP_E}{(1 + bP_E)^2} \end{aligned}$$

with $k'' = kabP_H$. This equation can be rearranged into a linear form [60] for a least-squares analysis to determine the parameters for the solid line in figure 15.

$$\left[\frac{P}{\text{rate}} \right]^{1/2} = \frac{b}{(kabP_H)^{1/2}} P_E + \frac{1}{(kabP_H)^{1/2}}$$

The fit in this case is rather poor. If it is assumed the ethylene adsorbs on a site different from the hydrogen adsorption site, the equation looks similar but without hydrogen and ethylene competing for the same sites, the divisor is not squared.

$$\text{rate} = k \left[\frac{aP_H}{1 + aP_H} \right] \left[\frac{bP_E}{1 + bP_E} \right]$$

$$\text{Rate} = k' \left[\frac{P_E}{1 + kP_E} \right]$$

with $aP_H \ll 1$ and $k' = kbaP_H$. The linear form is

$$\frac{\text{rate}}{k'P_E} = b - \frac{b}{k'} \text{ rate}$$

The excellent fit for this equation is shown in figure 16.

On a clean well-aligned single crystal surface, all metal atoms on the crystal faces are identical. Ethylene adsorbed on the clean surface to saturation coverage at room temperature inhibits hydrogen coadsorption [15,17,20,32] indicating adsorbed ethylene blocks hydrogen adsorption sites directly or sterically. Whether ethylene occupies the same site as hydrogen or blocks that site indirectly will result in a competitive adsorption treatment. In the second layer model of ethylene hydrogenation, hydrogen could adsorb on the bare spots on the metal surface while ethylene adsorbs on the first hydrocarbon adlayer. The second layer ethylene is sufficiently far from the surface to insure no carbon-hydrogen bonds are broken. The second layer ethylene is assumed to be weakly bonded to the first layer adspecies, the ethylene adsorption site. The possibility of either second layer or unique metal site adsorption-mechanism will be discussed in more depth after the TDS section.

The methane production increases with ethylene partial pressure (Figure 17) but the scatter in the data hinders a determination of the kinetic order. No breaking point in the plot is seen.

Effect of Oxygen

The effect of oxygen on the ethylene hydrogenation over iridium was determined in two ways. Two runs were performed with either five or ten torr oxygen in the feed. These two runs gave the same rates as runs without the oxygen added. In another trial the surface was heavily oxidized preceding the trial, but the rate was only reduced by a third.

Apparently any oxygen which is adsorbed by the surface rapidly reacts with either a hydrocarbon or hydrogen species to give water and carbon dioxide. These reactions are very rapid, do not leave any surface residue and do not change the ethylene hydrogenation rate.

A heavily oxidized surface did not lower the rate appreciably. An oxide covered surface does not poison ethylene hydrogenation completely. The reduction in the rate probably results from a reduced number of surface metal atoms.

Temperature Dependence

Figure 18 presents an Arrhenius plot (log turnover number versus T^{-1}) for $0.0016 < T^{-1} < 0.0032$ ($625\text{K} > T > 312\text{K}$). The plot is linear from $0.0025 < T^{-1} < 0.0032$ (400K

> T > 312K), and its slope in this region yields an activation energy of 12.5 Kcal/mole. The activation energy agrees favorably with other studies in this temperature range. From 500K to 623K the turnover number is approximately constant, but above 623K the ethylene hydrogenation rate after a short delay time was nonexistent in each trial, presumably because of ethylene decomposition and carbonization of the surface. The ethylene and hydrogen partial pressures were 0.45 and 70 torr respectively.

Methane production (Figure 19) did not show a maximum as a function of temperature in the Arrhenius plot, but a very slight break in the methane production turnover versus temperature plot (Figure 20) is more visible near the temperature of maximum hydrogenation. The Arrhenius energy below the break is 4.88 kcal/mole with little change noted if the entire temperature range is included.

Other studies have found an optimum temperature for ethylene hydrogenation [33] for a variety of metals in different forms. Over iridium films, Nagai and Miyahara [51] found an optimum temperature at 323K and Mahaffy et al. [57] working at lower temperatures discovered an optimum temperature at 190K. Mahaffy et al. found a portion of the ethylene adsorbed at 373K was dehydrogenated irreversibly. They believed this dehydrogenated species led to reduced rates by poisoning sites on the surface. Nagai and Miyahara

argued against this type of mechanism using mass balances of the reactants. They supported a change in the rate limiting step from hydrogen equilibrium to the formation of ethane. This study indicates the optimum temperature of ethylene hydrogenation is a result of a change in the form of adsorbed ethylene which is hydrogenated on the surface. This concept will be more fully developed following the TDS section.

Auger Results

Auger spectra were taken before almost every run. For a portion of the time period in which hydrogen kinetic order was under study, the Auger system was being repaired, and Auger spectra were not taken following runs. For all the ethylene and temperature dependence runs, Auger spectra were collected before and after the hydrogenation run. The ratio of the carbon-to-iridium peak-to-peak heights was used only to see trends in the carbon coverage. No attempt was made to calibrate these numbers to absolute coverages.

The Auger analysis of the crystal surface is done in high vacuum after an ethylene hydrogenation trial at pressures from the order of tenths to hundreds of torrs. Species adsorbed on the surface during reaction conditions may partially or completely desorb or change composition when the reactor is evacuated in preparation for the analysis. The crystal temperature is always lowered below

370K before evacuation below 100 millitorr. Only weakly adsorbed species will be pumped away leaving the more strongly adsorbed species to be measured by UHV techniques.

The carbon coverage after an ethylene hydrogenation trial increased slowly with the ethylene pressure for hydrogenation runs at 473K (Figure 21). The hydrogen dependence data (Figure 22) of the carbon coverage is limited and contains too much scatter to make any valid judgment of the trend. Zaera [15] found similar results for ethylene hydrogenation over platinum (111) between 300K to 370K. The carbon concentration did not depend on hydrogen pressure or temperature on platinum (111) under the limited conditions of Zaera's study.

The strongest trend in the relative carbon concentration occurred during the temperature dependence experiments (Figure 23). Up to 500K, the carbon coverage was fairly constant after each run, but above 500K the carbon coverage increased rapidly with the temperature of hydrogenation. The carbon concentration at 773K is ten times the carbon concentration at 500K.

Thermal Dehydrogenation Spectroscopy

After an ethylene hydrogenation run at 320K, the hydrogen thermal desorption spectrum (Figure 24) closely resembles the spectra seen from ethylidyne covered surfaces. The existence of ethylidyne on iridium (111) has been

verified in other studies [31]. A clear identification of the hydrogenated carbon adspecies left after ethylene hydrogenation as ethylidyne is not possible without further characterization. The possibility of this adspecies being ethylidyne is very likely considering the identification of ethylidyne on platinum (111) [15] after ethylene hydrogenation using TDS, LEED and HREELS.

To refer to the hydrogen thermal desorption peaks as desorption peaks is not quite correct. It is true hydrogen is desorbing from the surface at these temperatures but, as has been shown in the literature, these peaks are from the decomposition of a hydrogenated carbon adspecies to hydrogen atoms and a more dehydrogenated carbon adspecies. The hydrogen atoms, at the temperatures of the decomposition, react rapidly to form molecular hydrogen and then desorb. The actual temperature 373K [58] for chemisorbed hydrogen to desorb is much lower than the decomposition temperatures. The maxima in the hydrogen TD spectra indicate the temperatures at which the rates of decomposition of the hydrogenated surface adspecies (dehydrogenation) is at a maximum, not the temperature for maximum desorption of a pure hydrogen adspecies. The TD spectrum from ethylidyne on platinum (111) indicates dehydrogenation at 500K to a adspecies with a hydrogen for every carbon. This second adspecies dehydrogenates in a very wide temperature range as

seen in relatively broad second hydrogen TDS peak, 500K to 800K. The second adspecies is probably a mixture of more dehydrogenated hydrocarbon adspecies.

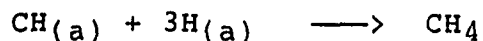
The sharp hydrogen TD peak indicates a single hydrogenated carbon adspecies with a sharp decomposition temperature. This first species establishes a definite surface concentration of carbon over a wide temperature range (Figure 23) as seen in the steady carbon concentration below 500K. It is only after its decomposition that higher surface concentrations of carbon are established. Engstrom et al. [59] measured the carbon concentration on iridium (111) and (110)-(1x2) after hydrogenolysis of several small hydrocarbons. They found one-fifth of a monolayer of carbon on the surface after ethane hydrogenolysis. Zaera [15] measured less than a half-monolayer of carbon after ethylene hydrogenation over platinum (111) from 300K to 373K. From these previous studies, the surface concentration of carbon is assumed to be less than a monolayer for temperatures below the first hydrogen TD peak, $\leq 500\text{K}$. The first ethylene derived adspecies does not completely cover the surface under hydrogenation conditions. It is either being hydrogenated and removed at a rate which prevents it from reaching a saturation coverage or it is in direct competition with hydrogen for surface sites.

The optimum temperature of ethylene hydrogenation agrees well with the expectations of Rye [50]. Rye proposed the decomposed ethylene fragments would poison further reaction. The hydrogen thermal decomposition spectrum taken after ethylene hydrogenation at 320K indicates a decomposition peak at the same temperature as the optimum temperature of ethylene hydrogenation seen over this surface (Figure 24). The higher temperature ethylene derived adspecies are being formed with the thermal decomposition of the first adspecies which coincides with the decrease in the rate of ethylene hydrogenation. The second broad TD peak starts to decline approximately at the temperature where hydrogenation activity ceases signifying complete dehydrogenation of the surface carbon adspecies with complete coking of the surface. Comparison of the Auger carbon/iridium peak-to-peak ratios after the temperature dependent hydrogenation runs with the hydrogen thermal desorption spectrum (Figure 25), indicates carbon buildup does not start to occur prior to the first decomposition peak. Carbon buildup appears as a very strong function of temperature above this point indicating strong carbonization of the surface is occurring with the decomposition of the high temperature adspecies.

If we assume the hydrogenation reaction is a strong function of the state of the adsorbed ethylene derived

adspecies, a change in the nature of these adspecies would be reflected in the activity of hydrogenation. In the extreme case, if the surface is completely covered with a layer of inert graphite, the reaction would cease completely. Arthur and Hansen reported graphite formation at 700K and in Figure 26, ethylene hydrogenation is seen to cease above 600K. The rapid multilayer carbon buildup above 550K is associated with graphite formation. On a carbon contaminated surface, ethylene hydrogenation shows a reduced rate. Similarly when the surface is covered with decomposed fragments of ethylene, the rate would be expected to be reduced.

At temperatures higher than the first dehydrogenation peak, these fragments of unknown structure populate the surface. One half of the available hydrogen is lost in the first TD peak to give the stoichiometry of the adspecies. They are not monocarbon adspecies as these fragments readily undergo complete and rapid hydrogenation to methane. The methane detected in the gas phase during ethylene hydrogenation originates from such a mechanism. The monocarbon units are removed as they are formed on the surface as methane.



The high temperature ethylene derived adspecies are partially hydrogenated dicarbon units with one or two

hydrogens. These weakly hydrogenated carbon species are difficult to hydrogenate and are possible precursors to coke formation.

The optimum temperature for ethylene hydrogenation is seen to be a function of the state of the partially dehydrogenated hydrocarbon overlayer. The optimum temperature for a particular metal can vary over a wide range [33]. The sensitivity of adsorbed ethylene to the surface structure can explain the deviations seen in the optimum temperature. The very stable ethylidyne is seen on Pt(111) but never on Pt(100). The field emission experiments indicate the transformations in the ethylene adlayer involving C-H and C-C bond breaking occur at higher temperatures on the (111) face than on the stepped (533) surface. The higher symmetry denser faces have dicarbon adspecies which are stable to higher temperatures than those on the other more open or less symmetric faces. The temperature range for the stability of the partially dehydrogenated dicarbon adspecies has direct bearing on the optimum temperature of ethylene hydrogenation.

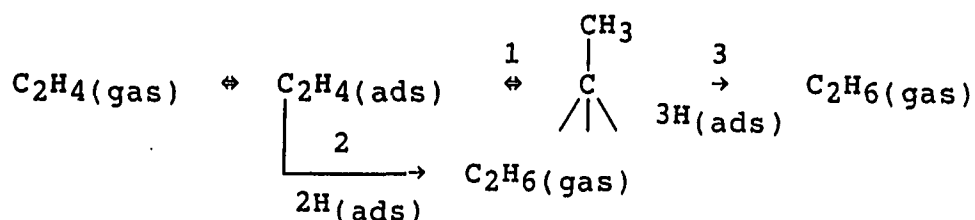
Many past investigators (see literature review) have proposed an ethylene hydrogenation mechanism which involves two layers of ethylene adsorption. They have proposed ethylene hydrogenation occurs on top of a layer of a strongly bound primary ethylene surface layer. The primary

adsorbed layer is not hydrogenated to a desorbable product during hydrogenation of gas phase ethylene. Strong evidence for this mechanism has been augmented by experiments using labeled ethylene. ^{14}C -ethylene is adsorbed creating a stable surface species prior to normal ethylene hydrogenation over this surface. The ^{14}C concentrations before and after ethylene hydrogenation are approximately equal supporting the existence of a stable primary layer on the surface during ethylene hydrogenation. Zaera and Somorjai have collected evidence supporting a primary layer composed of ethylidyne.

Coadsorption studies of ethylene and hydrogen cast doubt on this type of mechanism. If less than a Langmuir of ethylene is dosed on a hydrogen predosed surface, ethylene surface concentration is inversely proportional to the hydrogen predose amount [20]. The ethylene coverage reaches zero on a hydrogen saturated surface. Berkowitz et al. [20] have shown the TDS peak for ethylidyne decomposition shifts to lower temperatures with higher hydrogen precoverages and its intensity reduces. A concurrent increase in molecular ethylene and ethane desorption occurs also with a shift to lower temperature. Ethylidyne once formed hydrogenates more slowly than ethylene but the presence of adsorbed hydrogen inhibits ethylidyne formation. Beebe et al. [48] and Sheppard et al. [61] have shown under ethylene hydrogenation

conditions, ethylidyne is not formed if the hydrogen pressure is sufficiently high. Soma [19] found only 20% of the surface covered with ethylidyne during ethylene hydrogenation over many supported group VIII metals. This value is in agreement with ^{14}C -ethylene labeling studies by Norval et al. [47] on a similar set of supported catalysts showing retention of a fifth of a monolayer of strongly bound carbon after ethylene hydrogenation.

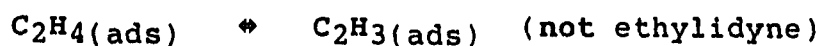
Beebe et al. [48] have illustrated the problem generally as,



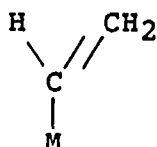
with rate 2 much greater than rates 1 and 3. This scheme appears to explain the observations of Mahaffy et al. [57]. They witnessed a drastic drop in the hydrogenation activity over an iridium thin film near 180K which is the temperature where ethylidyne is first observed on iridium (111). Mahaffy et al. believed a partially dehydrogenated ethylene adspecies was blocking sites reactive for hydrogenation.

Deuterium distribution studies represent a conflict with this scheme. The deuterium distribution in ethane from ethylene hydrogenation peaks at low deuterium content or has

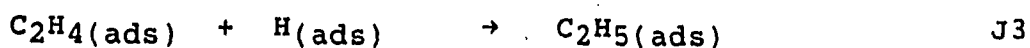
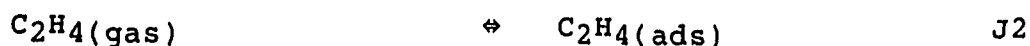
a horseshoe appearance peaking at low and high deuterium content depending on the catalyst and conditions. A mechanism involving hydrogenation of an associatively adsorbed ethylene species would not peak at high deuterium content. Another step must be introduced into this scheme to account for this observation.



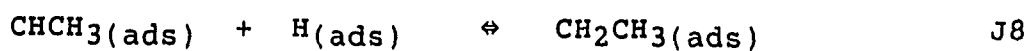
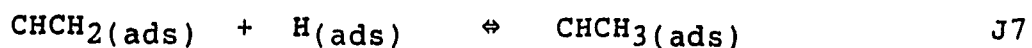
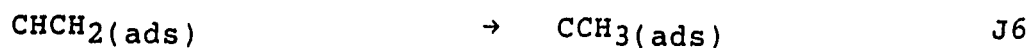
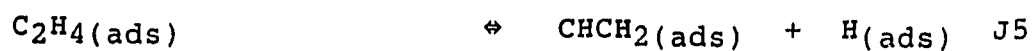
A possible structure for $\text{C}_2\text{H}_3(\text{ads})$ is a vinyl species, CHCH_2



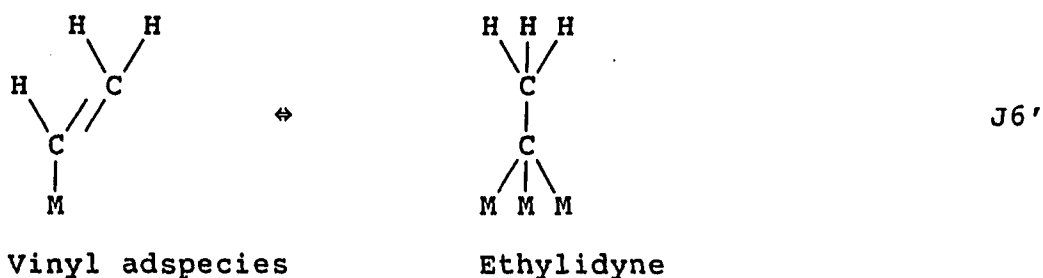
Below 200K, ethylene is di- σ -adsorbed and follows the simple mechanism,



where the hydrogen adsorption site is different than the ethylene adsorption site (see [39, 57] and ethylene dependence results). Above 200K where vinyl (CHCH_2) formation becomes important, some steps are added.



where step J5, the initial dehydrogenation of di- σ -adsorbed ethylene, was slow below 200K compared to step J3 but above 200K it is faster. The rearrangement of the vinyl species to ethylidyne is shown in step J6 more graphically below.



This step is slow compared to the hydrogenation of the vinyl species, step J7. In the presence of adsorbed hydrogen the vinyl species is hydrogenated before an appreciable amount of ethylidyne can be formed. If no adsorbed hydrogen is present as in the case of UHV ethylene adsorption studies, only ethylidyne is observed. The vinyl species is converted to ethylidyne quickly in the time scale of vacuum surface science probes. After ethylene hydrogenation, surface characterization with UHV techniques distinguished only ethylidyne. The vinyl adspecies rapidly reacts with the available hydrogen to form ethane and any remaining vinyl adspecies converts to ethylidyne, eliminating the vinyl species from the surface prior to surface characterization. These studies always report less than saturation carbon coverage, because of the removal of some ethylene derived adspecies during evacuation. In studies where the catalyst

surface composition is probed in the presence of the reacting gases, the ethylidyne concentration is kept to a minimum by the presence of hydrogen.

Step J4 is the rate limiting step above 200K giving a first order dependence in hydrogen. Below 200K the reverse of reaction J3 proceeds at a rate negligible compared to the rate of ethane production, so that J3 and J4 are both irreversible and at steady state ($\text{CH}_2\text{CH}_3(\text{ads})$ and C_2H_6 are produced at the same rate). This leads to the half order dependence in hydrogen pressure observed below 200K. As the temperature increases above 200K the first two hydrogenation steps of the surface intermediates, vinyl adspecies to ethylidene and ethylidene to ethyl adspecies, are in equilibrium. This results in the first order dependence of the hydrogenation rate on hydrogen pressure observed in the present work.

The ethylene dependence below 200K is zero [57] when di- σ -adsorbed ethylene reacts directly to give the ethyl adspecies. Above 200K, adsorbed ethylene will desorb or be converted to a vinyl adspecies which can react in equilibrium in steps J7 and J8 with hydrogen to give ethane. The desorption temperature of molecular ethylene is 110K [27] and at 180K [32] no molecular ethylene is observed on iridium (111). The ethylene desorption and conversion to the vinyl species are rapid. The vinyl and ethyl adspecies

concentrations are small as indicated by spectroscopic investigations performed during reaction [19, 48, 61]. The vinyl and ethyl adspecies equilibrium give rise to the second and fourth terms of the rate expression's divisor,

$$1 + \frac{K_{J5} P_E}{P_{H_2}^{1/2}} + K_{J7} P_E + K_{J4} P_E P_{H_2}^{1/2}$$

but the low concentrations of these adspecies permit the rate equation to be simplified to

$$\text{rate} = k_a P_{H_2} \left[\frac{b P_E}{1 + b P_E} \right]$$

Theoretical calculations and adsorption on mixed metal films [62] indicate hydrogen prefers to bond to several metal atoms. Ethynidyne is bonded to three metal atoms which is the probable site for hydrogen adsorption on face-centered cubic metals. The vinyl adspecies and the ethyl adspecies are bound to a single metal atom and ethylidene and di- σ -bonded ethylene are bound to two metal atoms. Except for ethynidyne, the ethylene derived adspecies adsorbs on sites different from those for adsorbed hydrogen. In sequential adsorption at room temperature, ethynidyne will block hydrogen adsorption. Berkowitz et al. [20] found ethylene desorbs at lower temperatures as ethane or ethylene if hydrogen is present on an adjacent site. If hydrogen is

not present, the ethylene is free to convert to ethylidyne and does not desorb. At low temperatures a ethylene predosed surface will release ethane when exposed to hydrogen.

Figure 27 illustrates the different temperature ranges of the various adsorbed ethylene derived species on iridium. The role each species plays on the ethylene hydrogenation mechanism is very sensitive to that species stability in a specified temperature range. The optimum temperature effect has been seen for other catalytic reactions and perhaps the change in the mechanism to give an optimum temperature is similar.

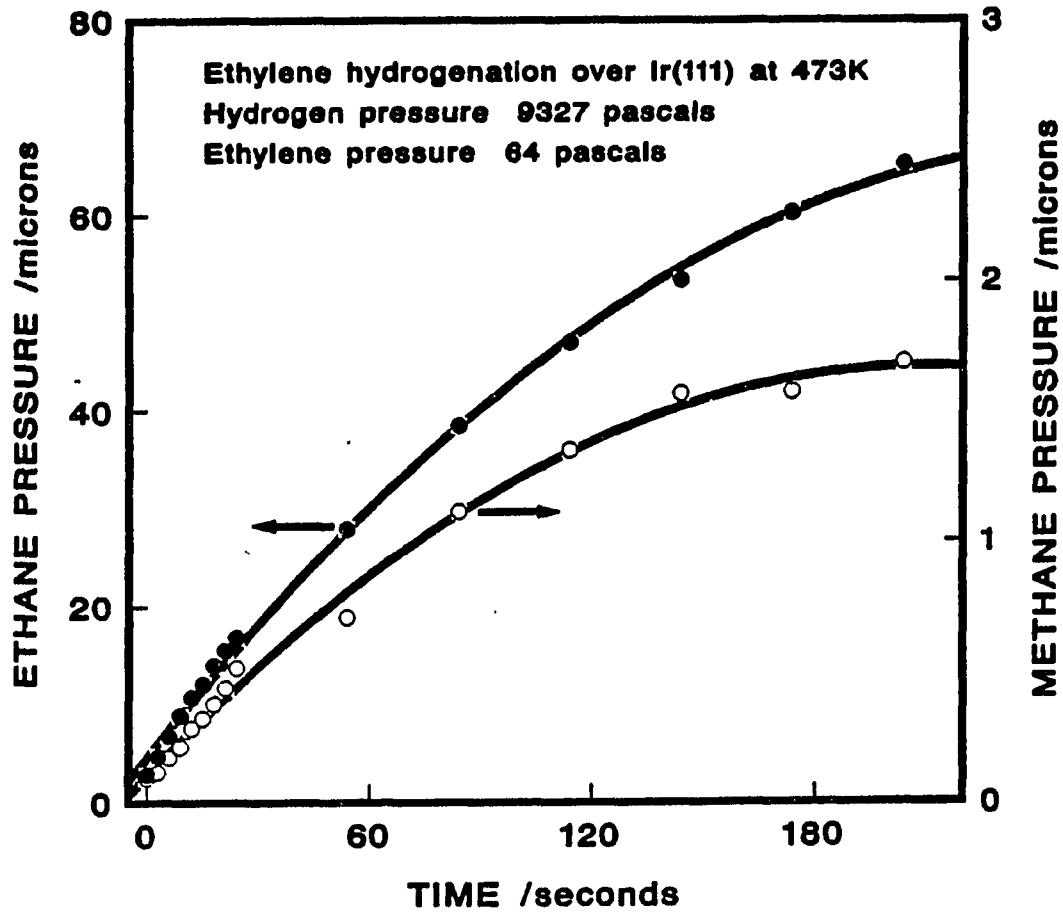


Figure 11. Example of an ethylene hydrogenation kinetic trial at 473K over iridium (111)

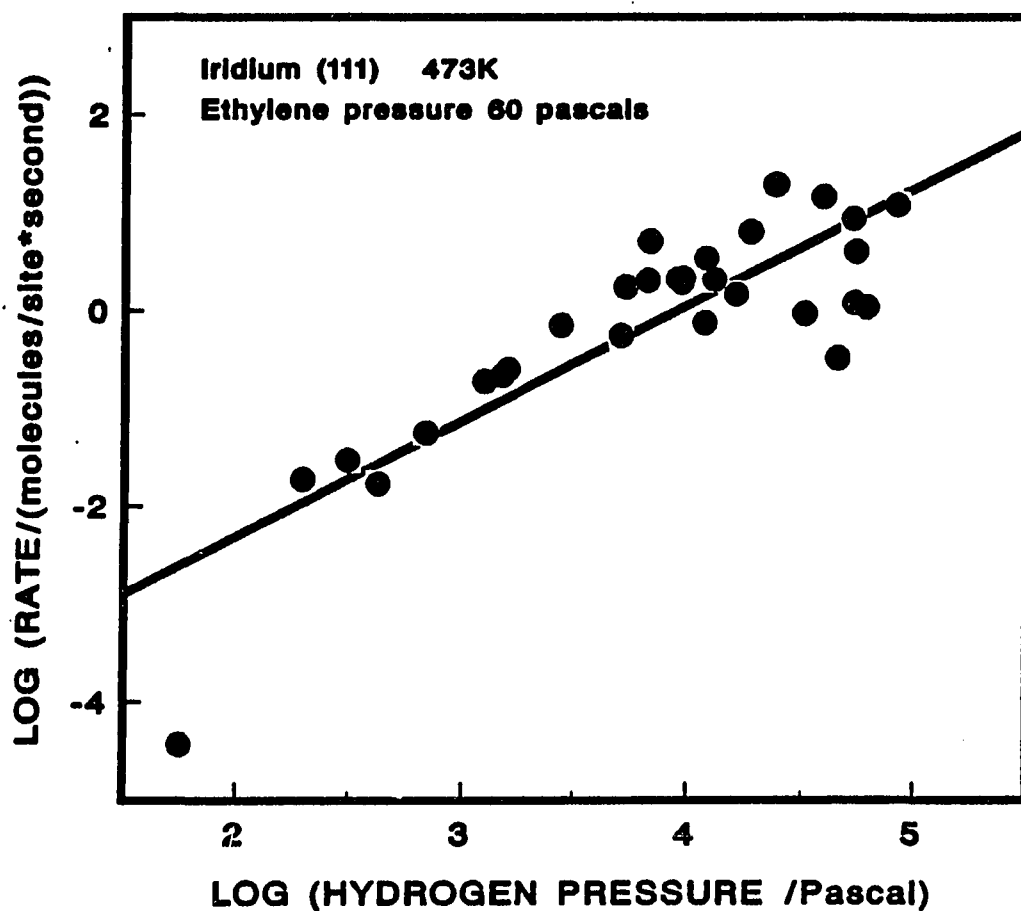


Figure 12. Hydrogen order plot of ethylene hydrogenation over iridium (111) at 473K. Individual initial rates are given as points and a least squares fit of the data is represented by the solid line with slope 0.98

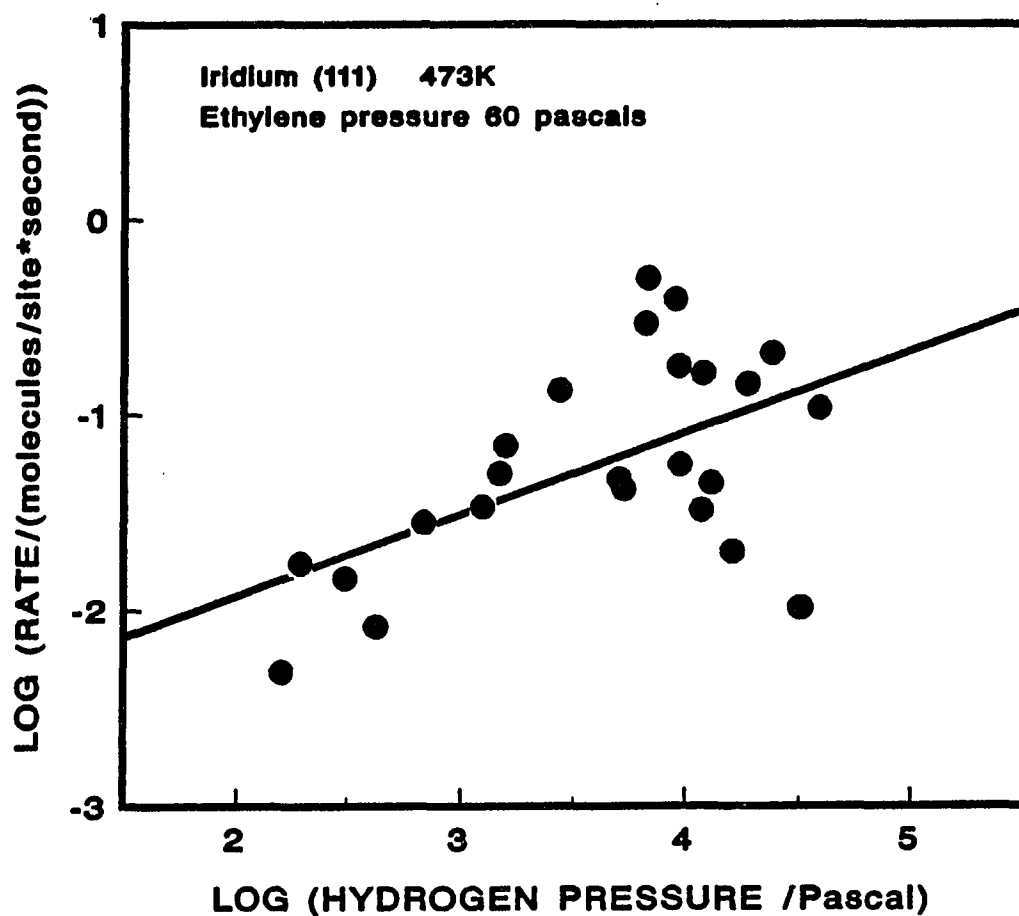


Figure 13. Hydrogen order plot of methane formation over iridium (111) at 473K. Individual initial rates are given as points and a least squares fit of the data is represented by the solid line

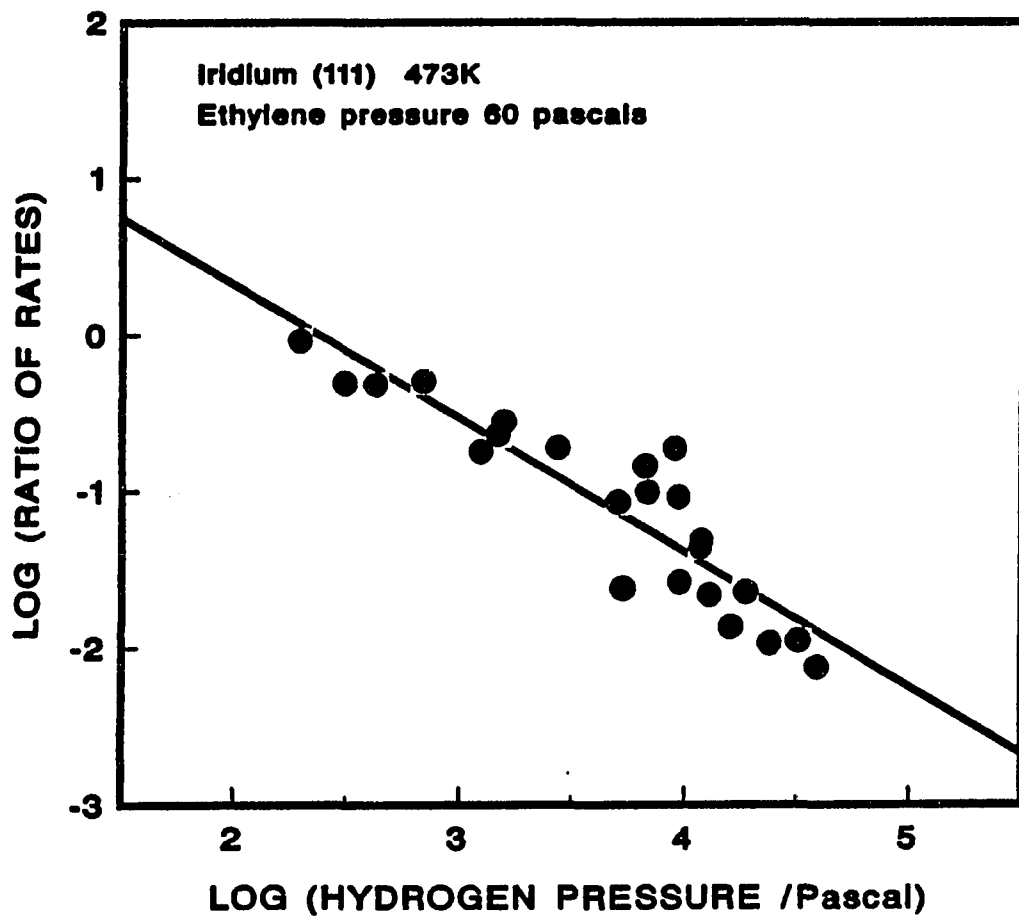


Figure 14. Ratio of the methane formation and hydrogenation initial rates as a function of hydrogen pressure

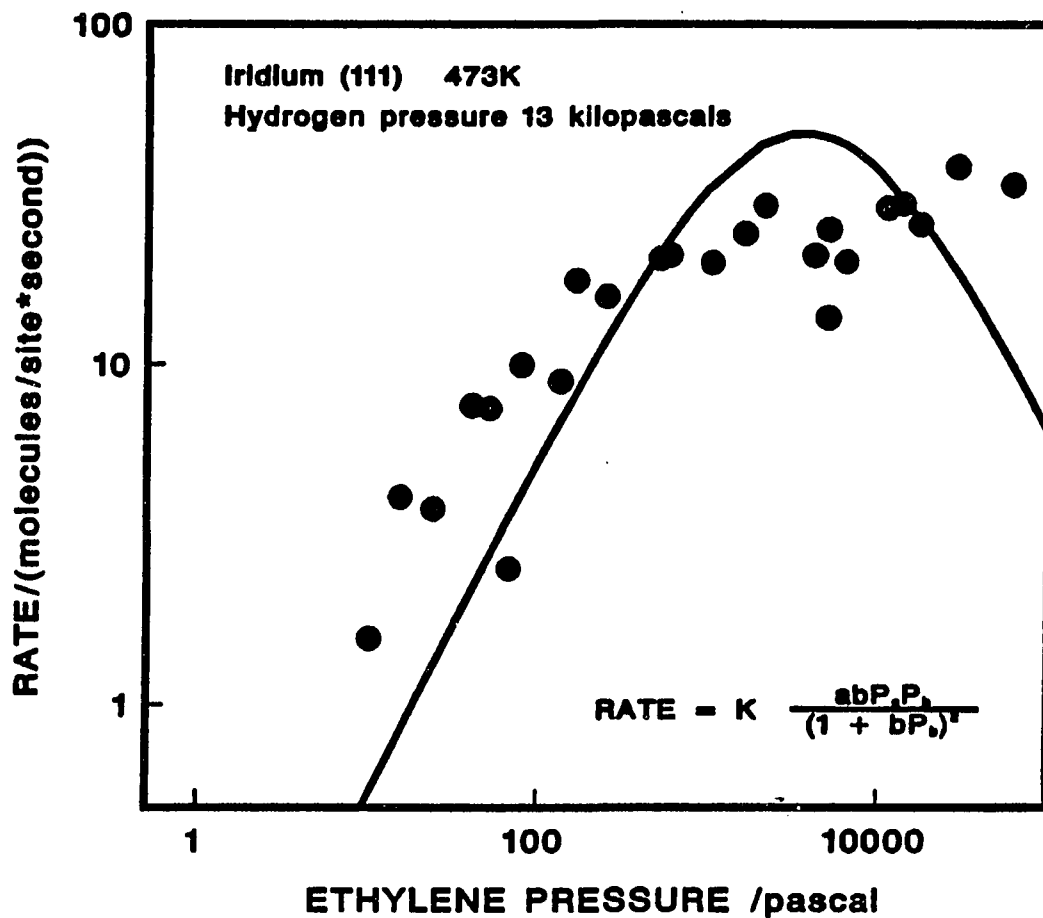


Figure 15. Fit of ethylene order plot data of ethylene hydrogenation over iridium (111) at 473K to competitive adsorption mechanism

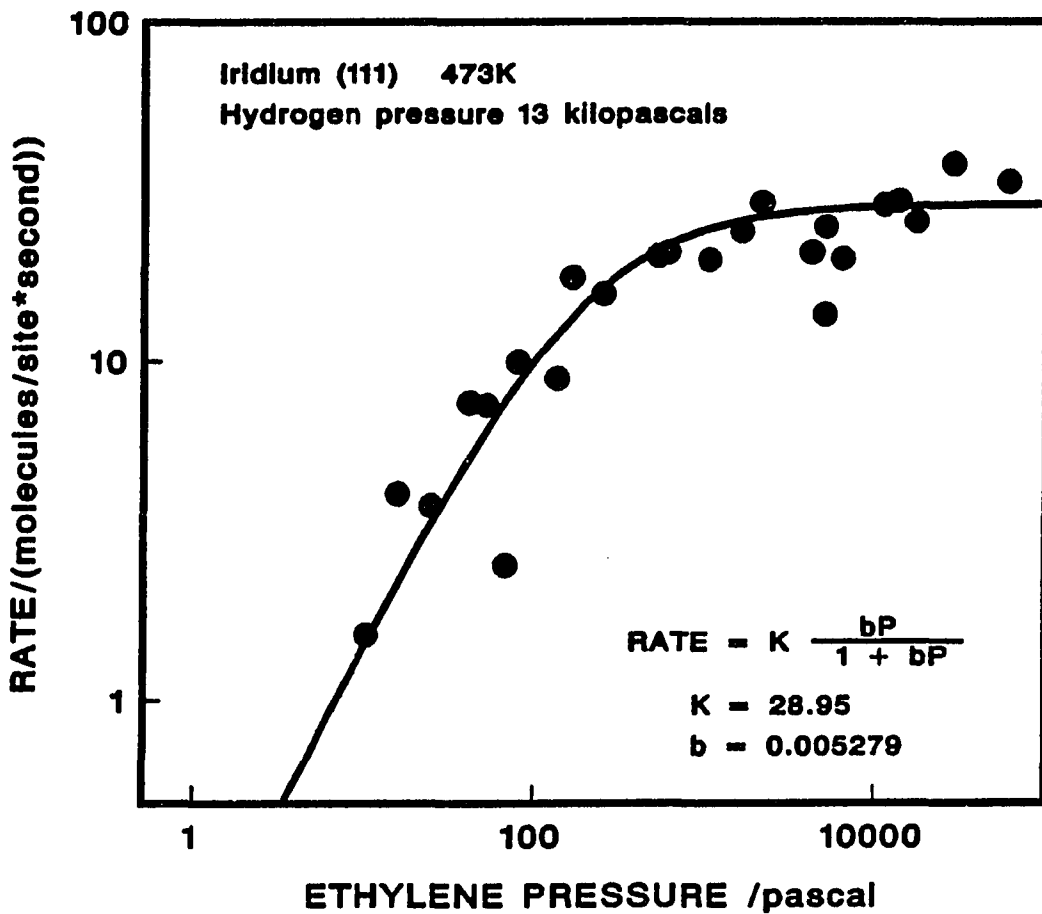


Figure 16. Fit of ethylene order plot data of ethylene hydrogenation over iridium (111) at 473K to two site mechanism

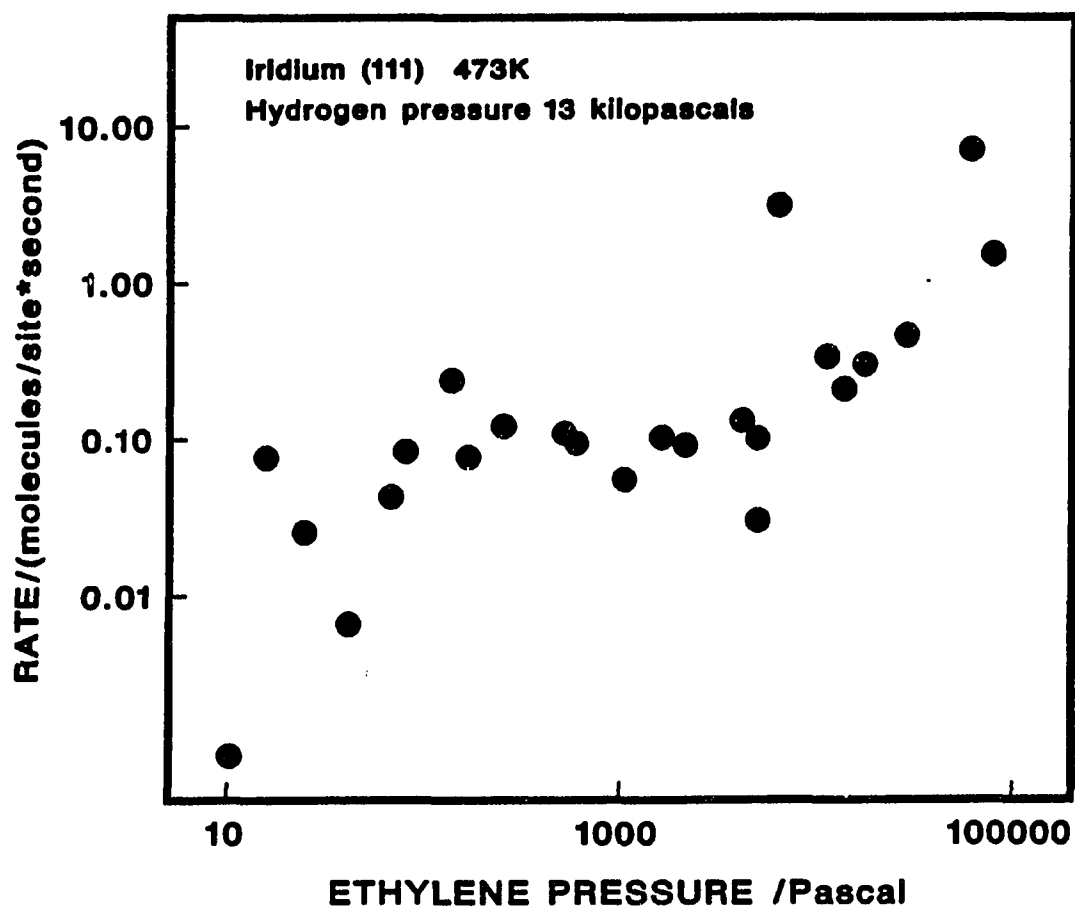


Figure 17. Ethylene order plot of methane formation over iridium (111) at 473K with 13 kilopascals hydrogen

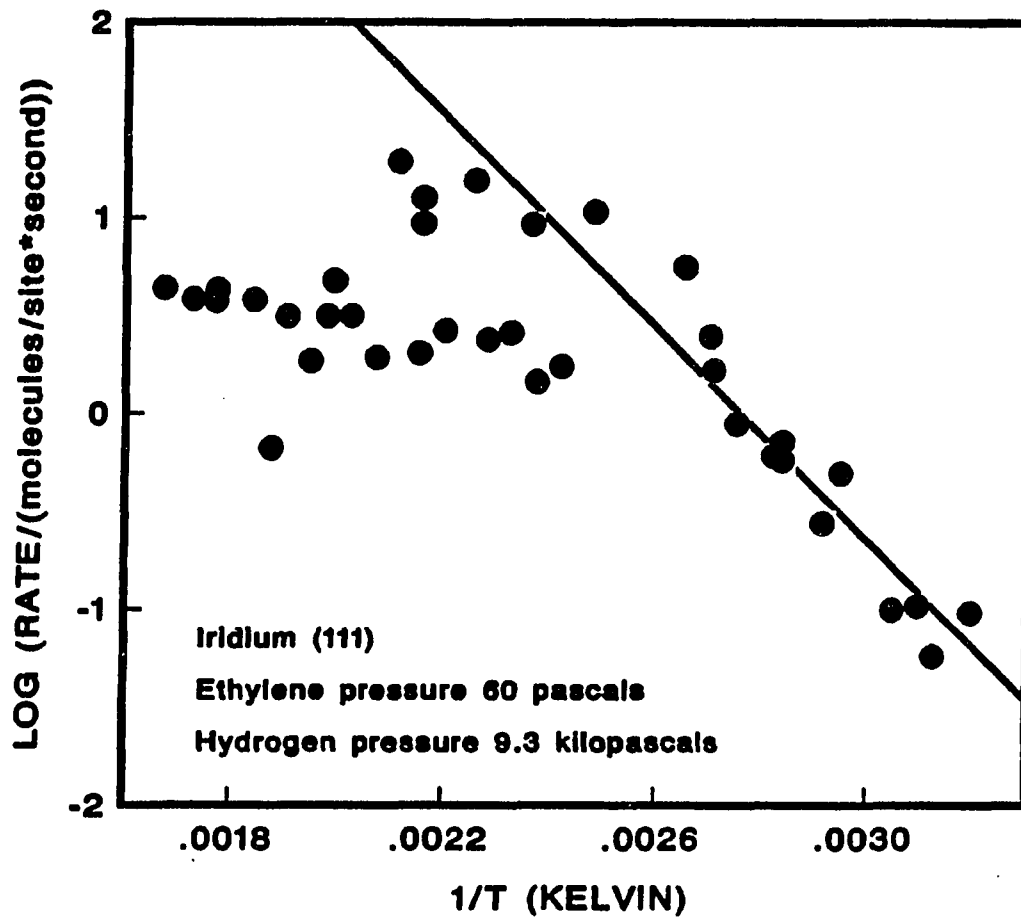


Figure 18. Arrhenius plot for ethylene hydrogenation over iridium (111) with a hydrogen pressure of 9333 pascals and ethylene pressure of 60 pascal (The solid line is a fit of low temperature data to give an activation energy of 12.5 Kcal/mole.)

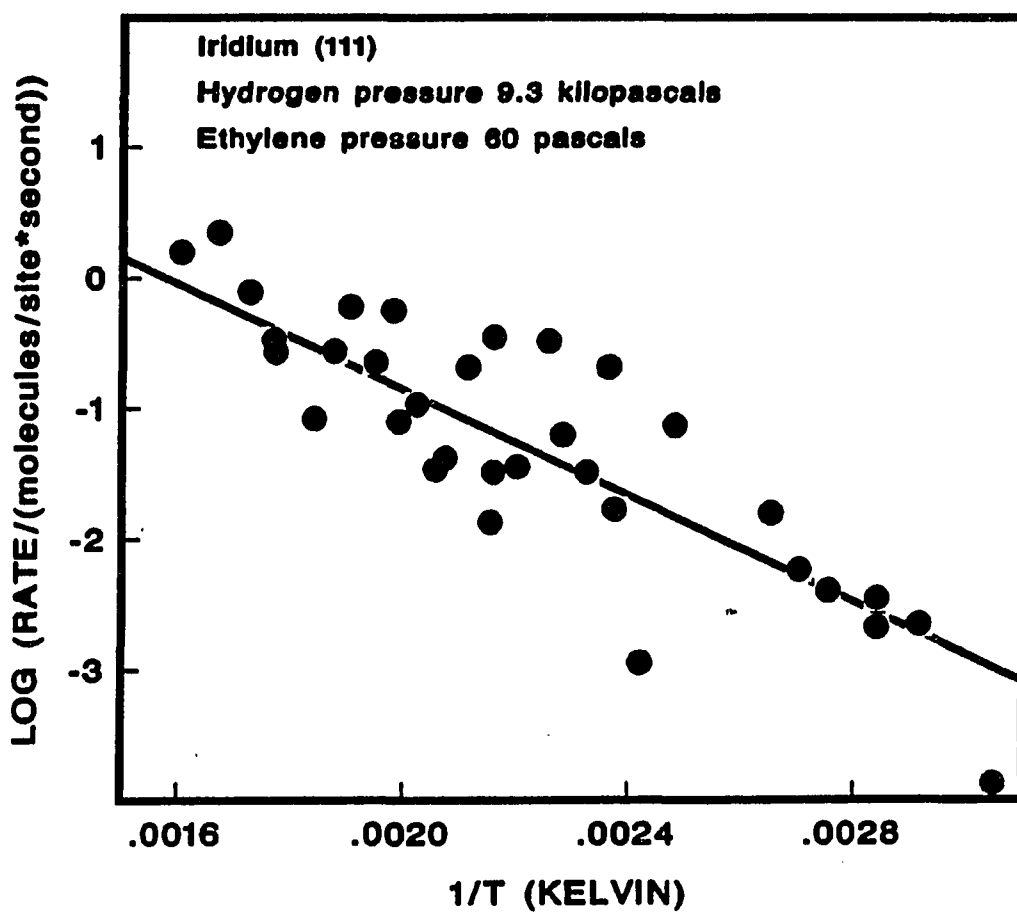


Figure 19. Arrhenius plot for methane formation over iridium (111) with a hydrogen pressure of 9333 pascals and ethylene pressure of 60 pascal (The solid line is a fit of the data to give an activation energy of 4.88 Kcal/mole.)

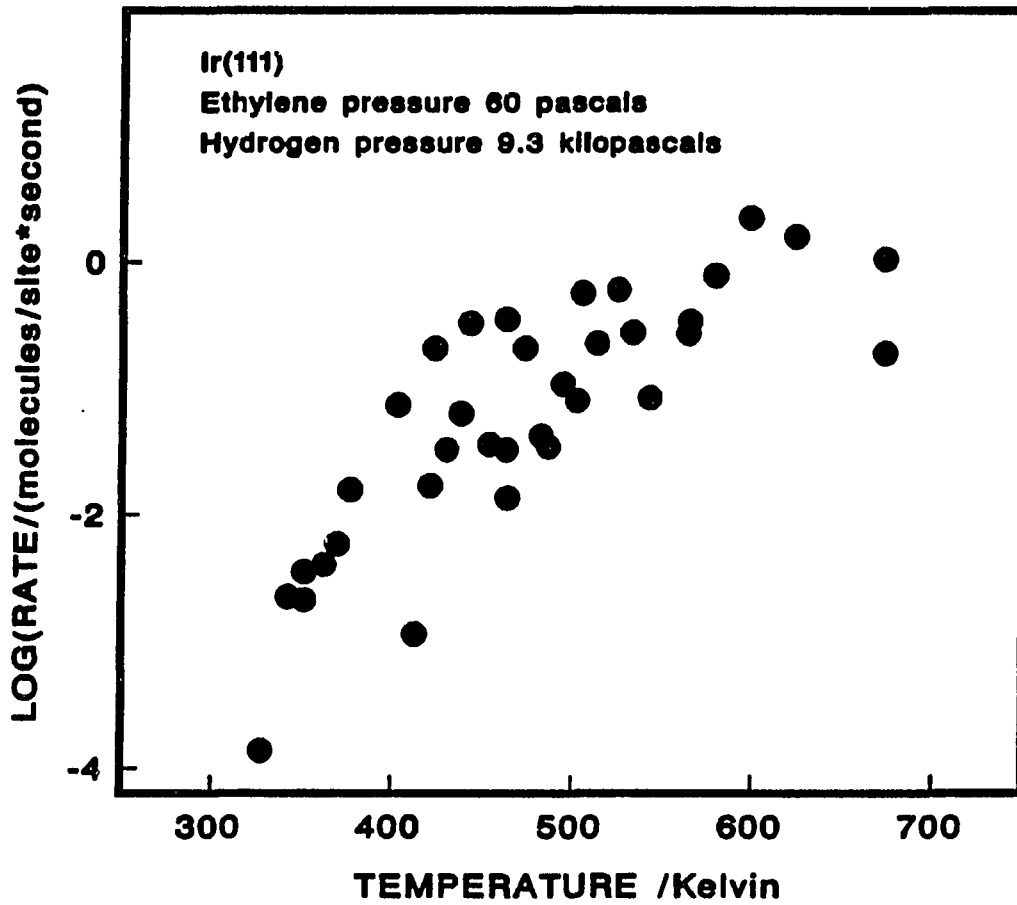


Figure 20. Methane formation as a function of temperature over iridium (111) with a hydrogen pressure of 9333 pascals and ethylene pressure of 60 pascal (Note the inflection around 500K.)

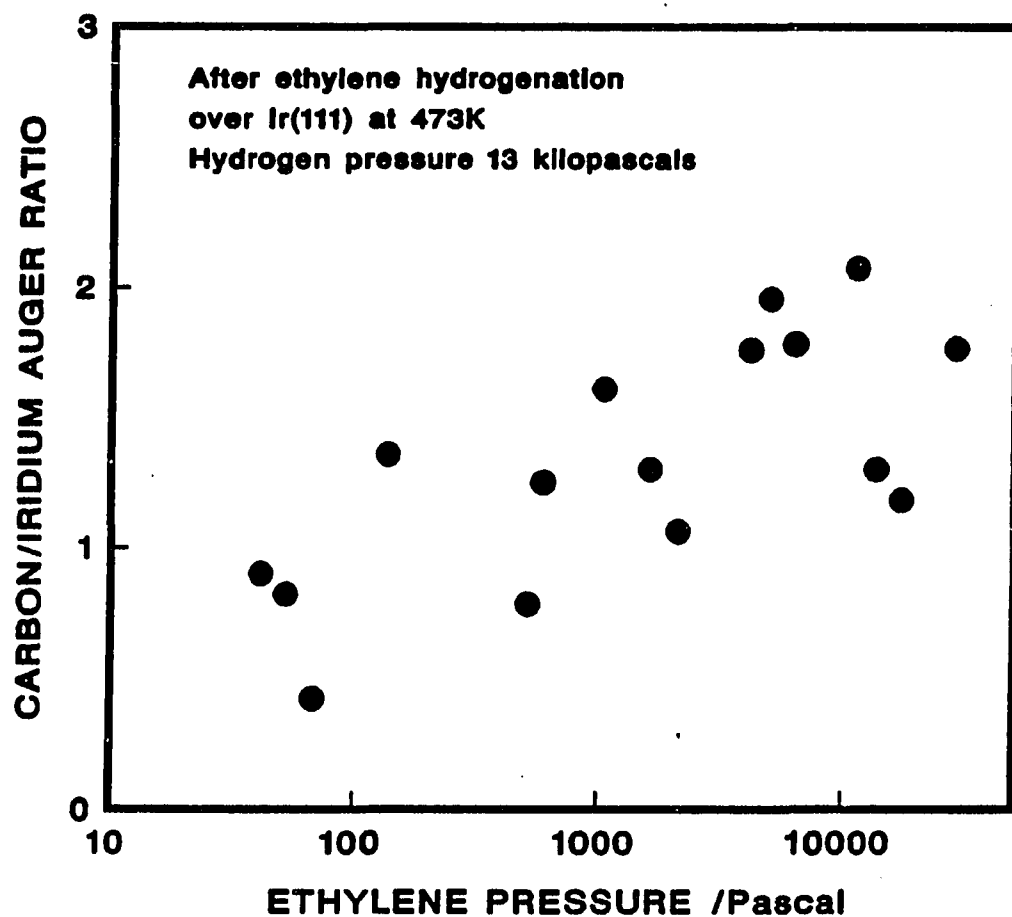


Figure 21. Ethylene pressure dependence of the carbon coverage after ethylene hydrogenation at 473K on iridium (111) and 13 kilopascals hydrogen derived from the ratio of the Auger peak-to-peak heights of carbon and iridium

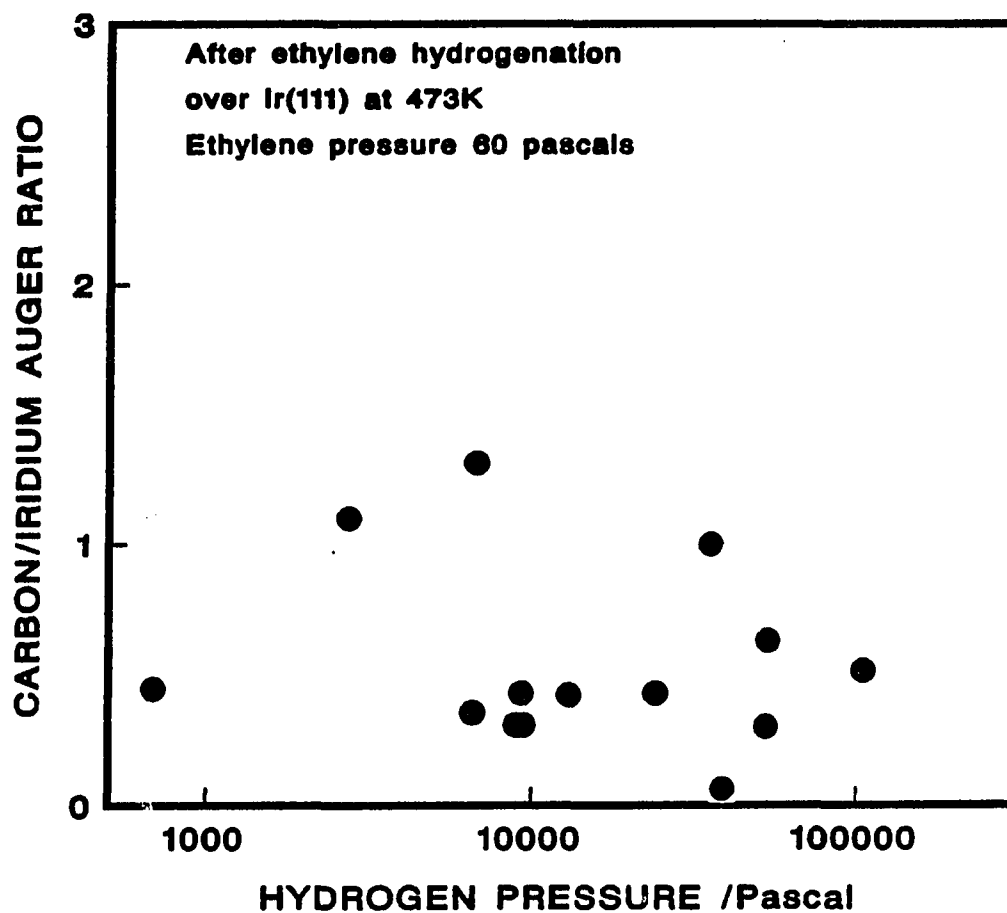


Figure 22. Hydrogen pressure dependence of the carbon coverage after ethylene hydrogenation at 473K on iridium (111) and 60 pascals ethylene derived from the ratio of the Auger peak-to-peak heights of carbon and iridium

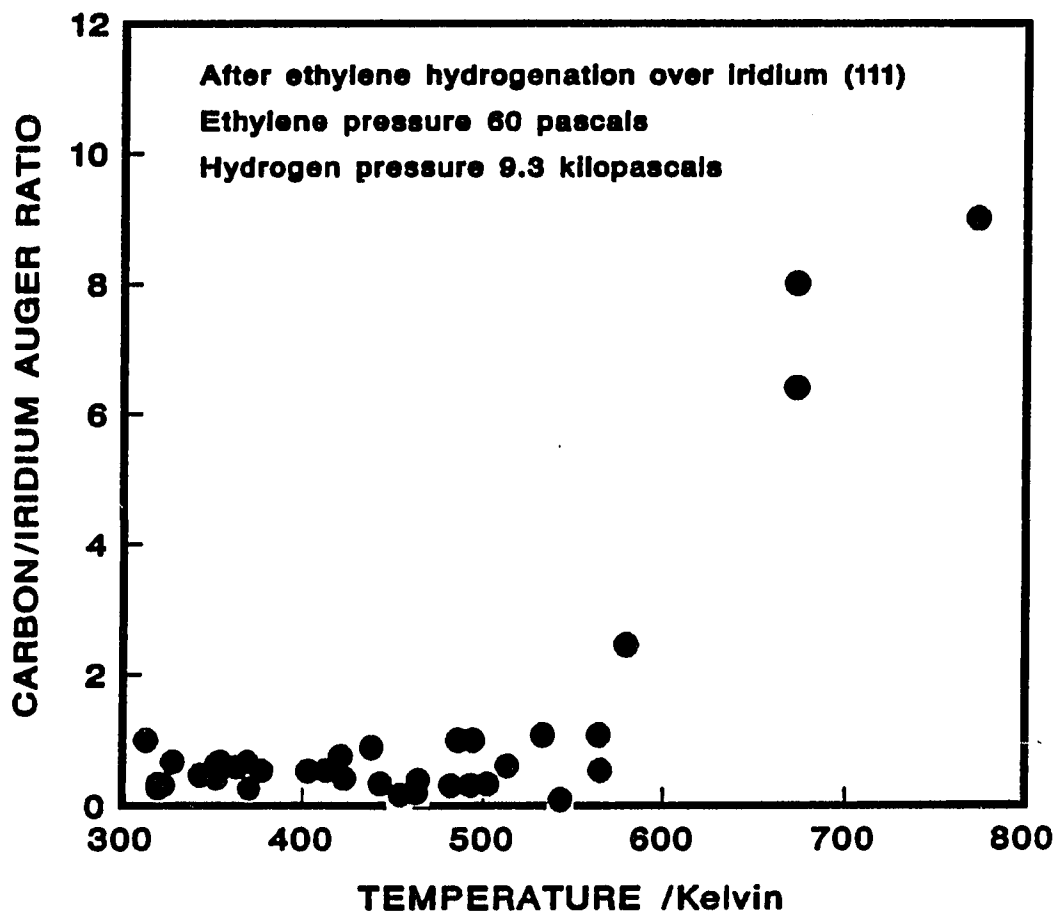


Figure 23. Temperature dependence of the carbon coverage after ethylene hydrogenation over iridium (111) with a hydrogen pressure of 9333 pascals and ethylene pressure of 60 pascal derived from the ratio of the Auger peak-to-peak heights of carbon and iridium

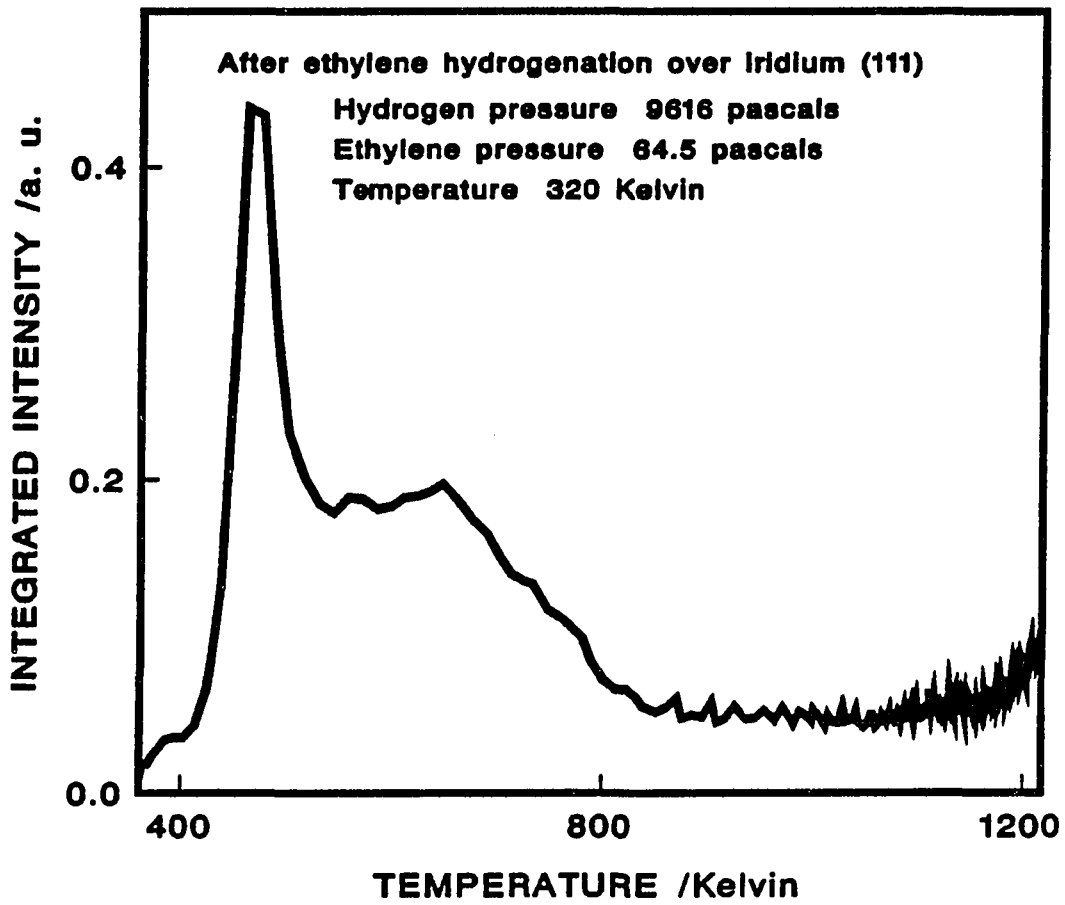


Figure 24. Hydrogen thermal desorption spectrum taken after ethylene hydrogenation over iridium (111) at 320K

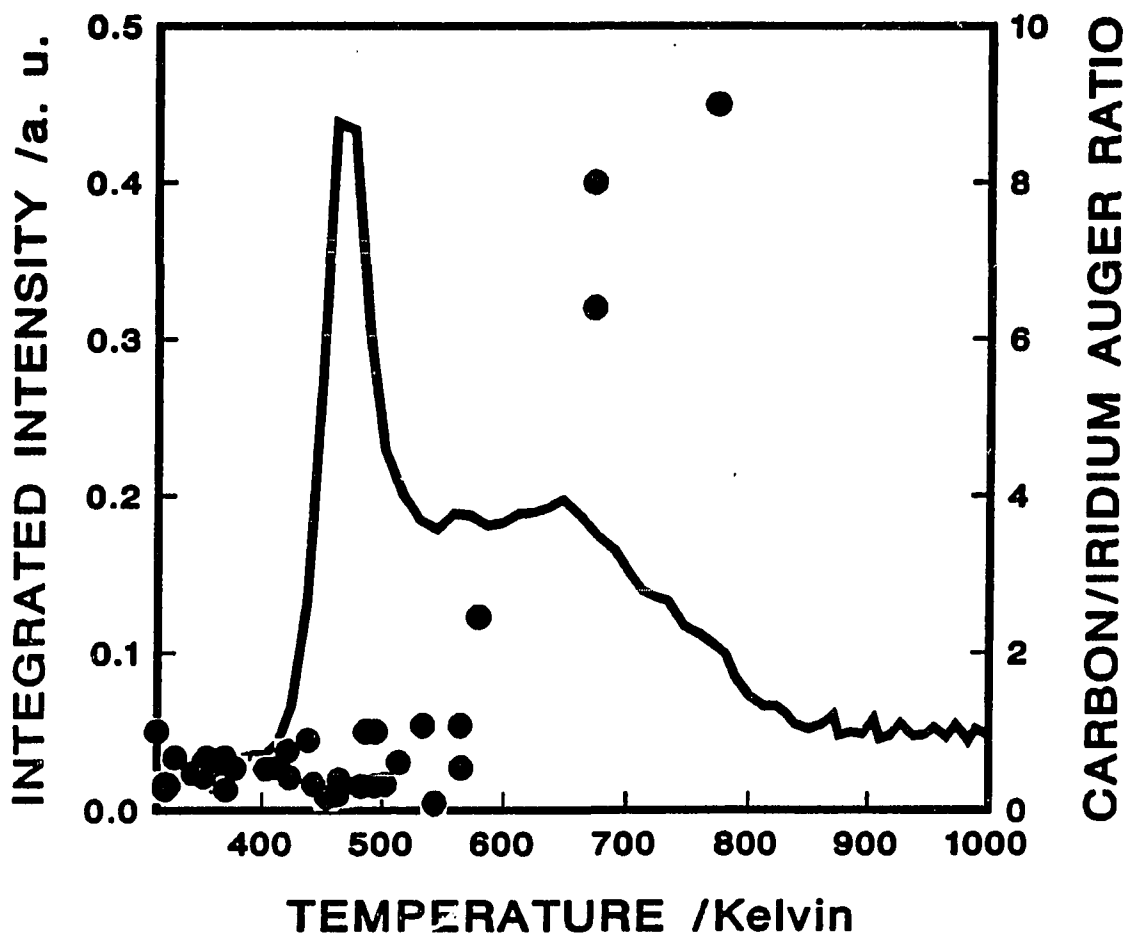


Figure 25. Hydrogen thermal desorption spectrum taken after ethylene hydrogenation over iridium (111) at 320K and the carbon coverage from Auger data as in Figure 24 superimposed

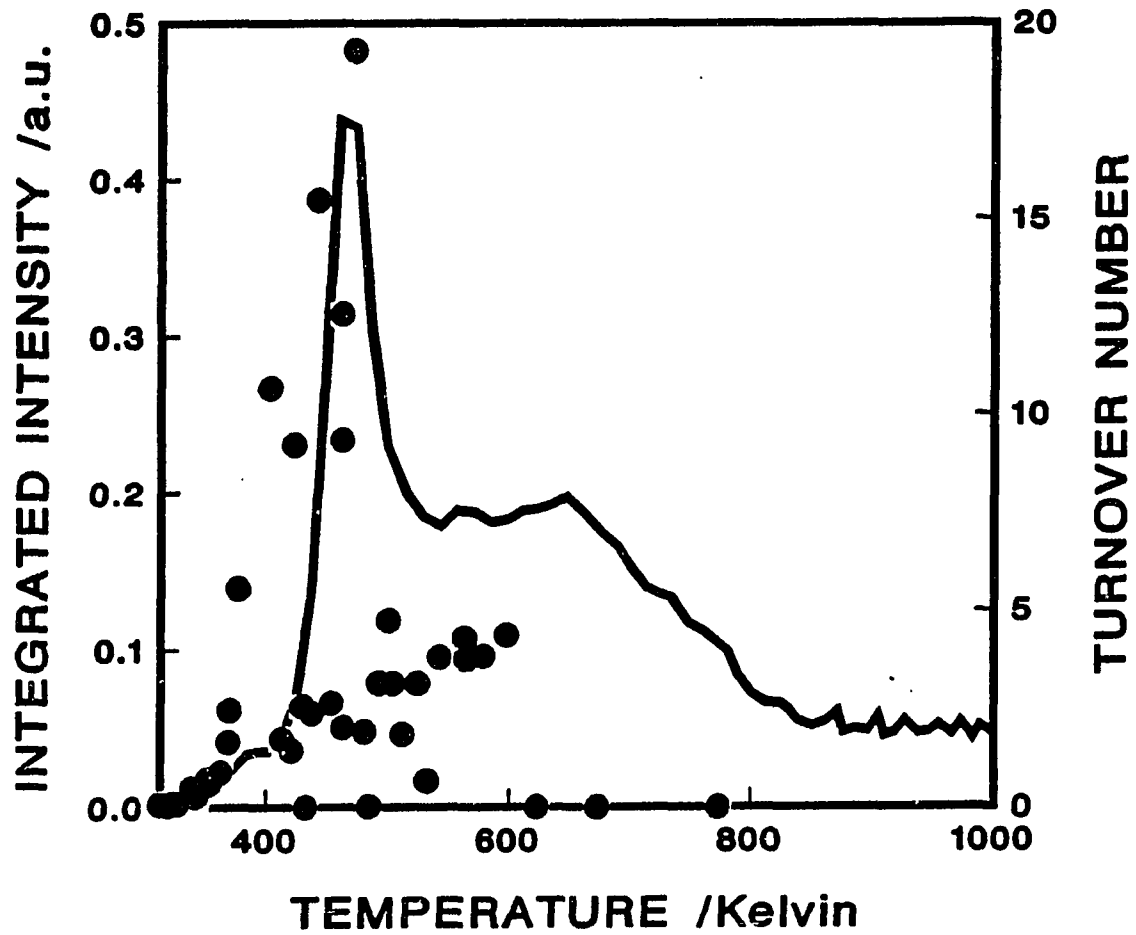


Figure 26. Hydrogen thermal desorption spectrum taken after ethylene hydrogenation over iridium (111) at 320K and the temperature dependence of ethylene hydrogenation initial rates superimposed

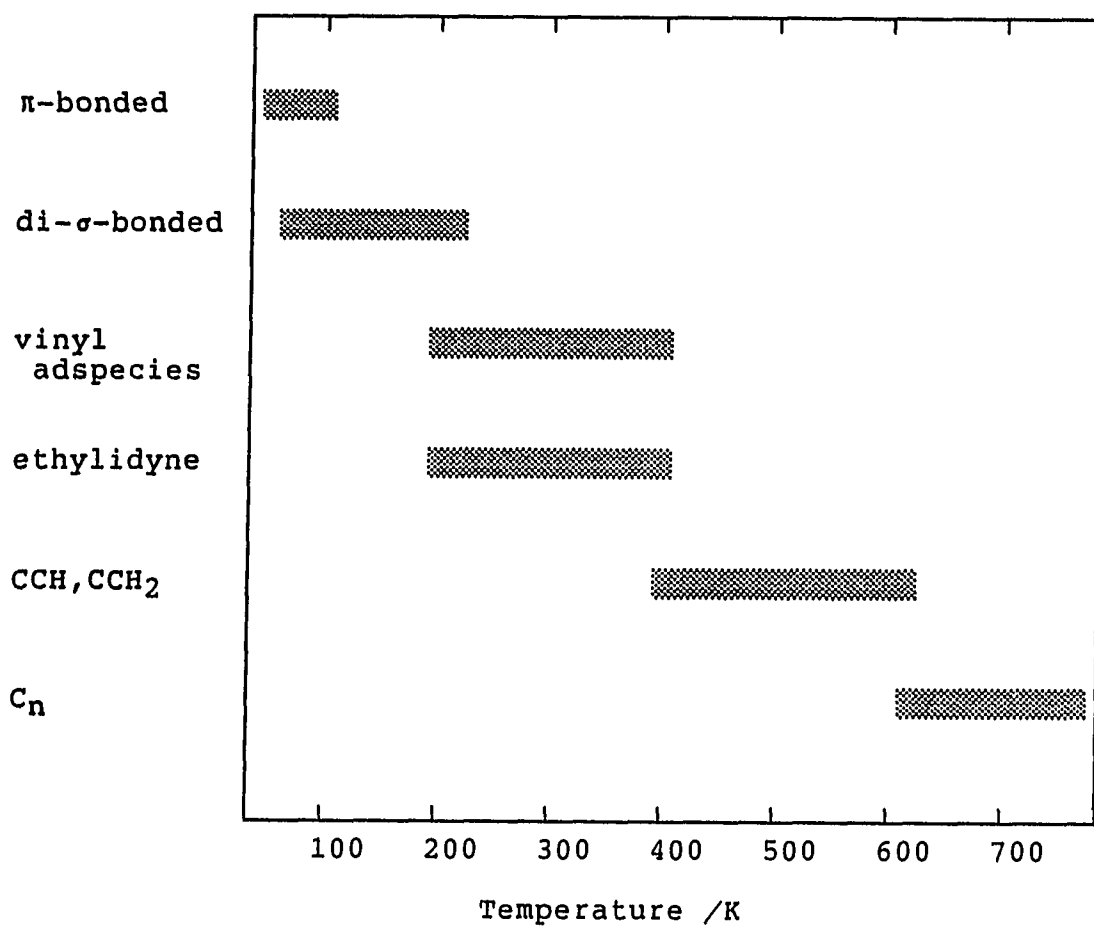


Figure 27. Approximate temperature ranges of stability of various ethylene derived adspecies found on iridium (111)

SUMMARY

A catalytic reactor with ultra-high vacuum analysis capabilities was designed and constructed to investigate the catalytic hydrogenation of ethylene over iridium (111). The small volume reactor operated as a continuously stirred batch reactor and can be evacuated to 10^{-8} torr. The reactor operates over a tremendous pressure range, 2000 torr to 10^{-3} torr. The catalyst can be heated to 1500K in vacuum or to 1000K under reaction conditions. Two methods of analyzing the partial pressures of gases in the reactor to determine initial rates are included in the reactor's design. Gas chromatography can accurately determine product partial pressures of a few microns in the presence of the reactant gases. A multiposition sampling valve and an all metal bellows recirculating pump decreased the time between sampling enabling the accurate determination of initial rates. A mass spectrometer can sample the gaseous environment of the reactor via a leak valve. A computer interface enables collection, quantification and storage of a large amount of mass spectral data.

A sample transfer system with a novel sealing system was designed to transfer the metal catalyst from the reactor to an ultra-high vacuum analysis chamber. The UHV chamber contains retarding field optics for LEED and Auger electron spectroscopy. Auger analysis provides accurate

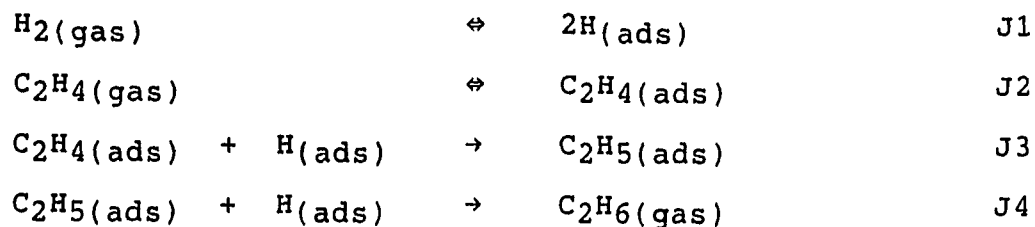
determination of surface cleanliness prior to a kinetic trial. Auger analysis after a kinetic trial can detect strongly bound surface species. Thermal desorption spectroscopy using the mass spectrometer-computer system characterizes volatile components on the surface after a kinetic trial.

The hydrogenation of ethylene has been investigated over iridium (111) single crystals in a uniquely designed catalytic reactor. Partial pressures of the reactants, hydrogen and ethylene, were varied from 10 to 10,000 pascals. The reaction was studied in the temperature range from 300K to 800K.

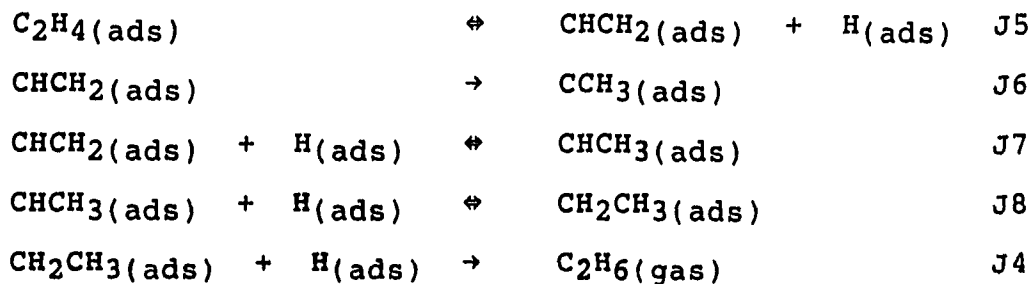
A rate equation was determined for ethylene hydrogenation at 473K over iridium (111).

$$\text{rate} = k_a P_{\text{H}_2} \left[\frac{b P_{\text{E}}}{1 + b P_{\text{E}}} \right]$$

Below 200K, ethylene is di- σ -adsorbed and follows the simple mechanism,



where the hydrogen adsorption site is different than the ethylene adsorption site. Above 200K where vinyl (CHCH_2) formation becomes important, some steps are added.



where step J5, the initial dehydrogenation of di- σ -adsorbed ethylene, was slow below 200K compared to step J3 but above 200K it is faster.

The reaction was first order in hydrogen and showed a Langmuir-Hinshelwood limiting behavior for ethylene dependence. Ethylene dependence at low pressures was first order. The derived kinetic equation suggests hydrogen and ethylene have different adsorption sites on iridium (111). The activation energy for ethylene hydrogenation between 312K and 625K is 12.5 kcal/mole.

Methane formation during ethylene hydrogenation was determined to originate from the hydrogenation of ethylene adspecies decomposition products and not from hydrogenolysis of ethane, the ethylene hydrogenation product. The methane formation increases with the partial pressure of either reactant. The activation energy is 4.9 kcal/mole.

Several correlations exist between the temperature dependencies of the concentration of strongly bound carbon adspecies, the ethylene hydrogenation rate and the thermal decomposition rates of adspecies on the surface after

ethylene hydrogenation. The optimum temperature of hydrogenation coincides with the first TDS peak. Decomposition of a kinetic intermediate partially poisons the surface altering its hydrogenation activity. More complete dehydrogenation of the surface adspecies is observed by a second TDS peak, an increase in the surface carbon concentration and complete deactivation of the surface for hydrogenation.

A mechanism is proposed and supported with experimental data and literature sources. The reason for an optimum temperature in the hydrogenation activity is suggested.

REFERENCES

1. Davis, S. M.; Somorjai, G. A. "The Chemical Physics of Solid Surfaces and Heterogeneous Catalysis ", King D. A.; Woodruff, D. P., Eds.; Elsevier: Amsterdam, 1982; Vol. 4, Chapter 7.
2. Bertolini, J. C.; Massardier, J. In "The Chemical Physics of Solid Surfaces and Heterogeneous Catalysis", King, D. A.; Woodruff, D. P., Eds.; Elsevier: Amsterdam, 1984; Vol. 3B, Chapter 2.
3. a) Kang, D. B.; Anderson, A. B. Surf. Sci. 1985, 155, 639-52.
b) Tysoe, W. T.; Nyberg, G. L.; Lambert, R. M. J. Phys. Chem. 1984, 88, 960-3.
4. a) Stuve, E. M.; Madix, R. J. J. Phys. Chem. 1985, 89, 3183-5.
b) Stuve, E. M.; Madix, R. J. Surf. Sci. 1985, 160, 293-304.
c) Stuve, E. M.; Madix, R. J. J. Phys. Chem. 1985, 89, 105-12.
d) Stuve, E. M.; Madix, R. J.; Brundle, C. R. Surf. Sci. 1985, 152/153, 532-42.
e) Stuve, E. M.; Jorgensen, S. W.; Madix, R. J.
'Oxygen Interactions and Reactions on
Palladium(100): Coadsorption Studies with C₂H₄,

- H₂O, and CH₃OH', In "Catalyst Characterization Science: Surface and Solid State Chemistry"; Deviney, M. L.; Gland, J. L., Eds.; American Chemical Society: Washington, D. C., 1985.
5. Ponec, V. In "The Chemical Physics of Solid Surfaces and Heterogeneous Catalysis", King, D. A.; Woodruff, D. P., Eds.; Elsevier: Amsterdam, 1982; Vol. 4, Chapter 8.
 6. Webb, G. In "Catalysis (Specialist Periodic Reports)", Kemball, C., Ed.; The Chemical Society: London, 1977; Vol. II, Chapter 6.
 7. Van Broekhoven, E. H.; Ponec, V. Prog. Surf. Sci. 1985, 19, 351-400.
 8. Webb, G. In "Chemical Kinetics ", Bamford, C. H.; Tipper, C. F. H., Eds; Elsevier: New York, 1978; Vol. 20, Chapter 1.
 9. Kemball's work is reviewed in Bond, G. C. "Catalysis by Metals"; Academic Press: London, 1962, Chapter 9.
 10. Steininger, H.; Ibach, H.; Lehwald, S. Surf. Sci. 1982, 117, 685-98.
 11. Ibach, H.; Hopster, H.; Sexton, B. Appl. Surf. Sci. 1977, 1, 1-24.
 12. a) Demuth, J. E. Surf. Sci. 1979, 80, 367-87.
b) Demuth, J. E. Surf. Sci. 1980, 93, L82-8.
 13. Kesmodel, L. L.; Gates, J. A. Surf. Sci. 1981, 111, L747-54.

14. Skinner, P.; Howard, M. W.; Oxton, I. A.; Kettle, S. F. A.; Powell, D. B.; Sheppard, N. J. J. Chem. Soc., Faraday Trans. 2 1981, 77, 1203.
15. Zaera, F. Ph.D. Dissertation, University of California, Berkeley, California, 1984.
16. Godbey, G.; Zaera, F.; Yeates, R.; Somorjai, G. A. Surf. Sci. 1986, 167, 150-66.
17. Davis, S. M.; Zaera, F.; Gordon, B. E.; Somorjai, G. A. J. Catal. 1985, 92, 240-6.
18. Zaera, F.; Somorjai, G. A. J. Amer. Chem. Soc. 1984, 106, 2288-93.
19. a) Soma, Y. J. Catal. 1979, 59, 239-47.
b) Soma, Y. J. Catal. 1982, 75, 267-7.
20. Berlowitz, P.; Megiris, C.; Butt, J. B.; Kung, H. H. Langmuir, 1986, 1, 206-12.
21. Van Strien, A. J.; Nieuwenhuys, B. E. Surf. Sci. 1979, 80, 226.
22. Kojima, I.; Miyazaki, E.; Yasumori, I. Appl. Surf. Sci. 1982, 10, 27-41.
23. a) Sinfelt, J. H. Catal. Rev. 1969, 3, 175-205.
b) Sinfelt, J. H. Adv. Catal. 1973, 23, 91-119.
c) Sinfelt, J. H. Catal. Rev. Sci. Eng. 1974, 9, 147-68.
d) Sinfelt, J. H. Rev. Mod. Phys. 1979, 51, 569-89.
24. Demuth, J. E.; Ibach, H.; Lehwald, S. Phys. Rev. Lett. 1978, 40, 1044.

25. Dubois, L. H.; Castner, D. G.; Somorjai, G. A. J. Chem. Phys. 1980, 72, 5234-40.
26. Hills, M. M.; Parameter, J. E.; Mullins, C. B.; Weinberg, W. H. J. Amer. Chem. Soc. 1986, 108, 3554-62.
27. Hansen, R. S.; Arthur, J. R. Jr.; Mimeault, V. J.; Rye, R. R. J. Phys. Chem. 1966, 70, 2787-92.
28. a) Nieuwenhuys, B. E.; Hagen, D. I.; Rovida, G.; Somorjai, G. A. Surf. Sci. 1976, 59, 155-76.
b) Nieuwenhuys, B. E.; Somorjai, G. A. Surf. Sci. 1978, 72, 8-32.
29. Arthur, J. R. Jr.; Hansen, R. S. J. Chem. Phys. 1962, 36, 2062-71.
30. Witt, J.; Nieuwenhuys, B. E. Surf. Sci. 1982, 119, 1-9.
31. Niemantsverdriet, J. W.; Van Langeveld, A. D. Fuel 1986, 65, 1396-8.
32. Marinova, Ts. S.; Kostov, K. L. Surf. Sci. 1987, 181, 573-85.
33. This mechanism is fully discussed in Horiuti, J.; Miyahara, K. 'Hydrogenation of Ethylene on Metallic Catalysts', "National Bureau of Standards Reference Data Series 13", 1968.
34. Farkas, A.; Farkas, L. J. Amer. Chem. Soc. 1938, 60, 1164-72.
35. Twigg, G. H.; Rideal, E. K. Proc. Royal Soc. 1939, A171, 55-69.

36. Jenkins, G. I.; Rideal, E. K. J. Chem. Soc. 1955, 2490-2500.
37. Wagner, C.; Hauffe, K. Zeit. Electro. 1939, 45, 409-25.
38. Taylor, H. A.; Thon, N. J. Amer. Chem. Soc. 1953, 75, 2747-50.
39. Mahaffy, P. Ph.D. Dissertation, Iowa State University, Ames, Iowa, 1977.
40. Bond, G. C. "Catalysis by Metals"; Academic Press: New York, N. Y., 1962.
41. Gardner, N. C.; Hansen, R. S. J. Phys. Chem. 1970, 74, 3298-9.
42. Thomson, S. J.; Webb, G. J. Chem. Soc., Chem. Commun. 1976, 526-7.
43. a) Reid, J. U.; Thomson, S. J.; Webb, G. J. Catal. 1973, 29, 421-32.
b) Reid, J. U.; Thomson, S. J.; Webb, G. J. Catal. 1973, 29, 433-40.
c) Reid, J. U.; Thomson, S. J.; Webb, G. J. Catal. 1973, 30, 372-7.
44. Weinberg, W. H.; Deans, H. A.; Merrill, R. P. Surf. Sci. 1974, 41, 312.
45. a) Al-Ammar, A. S.; Webb, G. J. Chem. Soc., Faraday Trans. I 1978, 74, 195-205.
b) Al-Ammar, A. S.; Webb, G. J. Chem. Soc., Faraday Trans. I 1978, 74, 657-64.

- c) Al-Ammar, A. S.; Webb, G. J. Chem. Soc., Faraday Trans. I 1979, 75, 1900-11.
46. a) Dus, R. Surf. Sci. 1975, 50, 241-52.
b) Dus, R.; Lisowski, W. Surf. Sci. 1979, 85, 183-99.
47. Norval, S. V.; Thomson, S. J.; Webb, G. Appl. Surf. Sci. 1980, 4, 51-81.
48. a) Beebe, T. P. Jr.; Albert, M. R.; Yates, J. T. Jr. J. Catal. 1985, 96, 1-11.
b) Beebe, T. P. Jr.; Yates, J. T. Jr. J. Amer. Chem. Soc. 1986, 108, 663-71.
49. a) Sato, S. J. Res. Inst. Catal., Hokkaido Univ. 1976, 24, 127-47.
b) Sato, S.; Miyahara, K. J. Res. Inst. Catal., Hokkaido Univ. 1975, 23, 17-25.
c) Sato S.; Miyahara, K. J. Res. Inst. Catal., Hokkaido Univ. 1975, 23, 1-16.
50. Rye, R. J. Res. Inst. Catal., Hokkaido Univ. 1969, 17, 223-7.
51. Nagai, K.; Miyahara, K. J. Res. Inst. Catal., Hokkaido Univ. 1970, 18, 183-8.
52. Miyahara, K.; Oki, S.; Harada, K.; Nagai, K. J. Res. Inst. Catal., Hokkaido Univ. 1968, 16, 555-66.
53. Honda, T.; Otsuka, K.; Mardaleishvilli, R. E. J. Chem. Soc., Japan 1969, 90, 1093-6.
54. Wendelken, J. F.; Withrow S. P.; Foster, C. A. Rev. of Sci. Instrum. 1977, 48, 1215-6.

55. Wood, E. A. "Crystal Orientation Manual"; Columbia University Press: New York, 1963.
56. Bond, W. L. "Crystal Technology"; John Wiley and Sons: New York, 1976.
57. Mahaffy, P.; Masterson, P. B.; Hansen, R. S. J. Chem. Phys. 1976, 64, 3911-6.
58. Engstrom, J. R.; Tsai, W.; Weinberg, W. H. J. Chem. Phys., in press.
59. a) Engstrom, J. R.; Goodman, D. W.; Weinberg, W. H. J. Amer. Chem. Soc. 1986, 108, 4653-5.
b) Engstrom, J. R.; Goodman, D. W.; Weinberg, W. H. J. Amer. Chem. Soc., submitted.
c) Engstrom, J. R.; Goodman, D. W.; Weinberg, W. H. J. Phys. Chem., submitted.
60. Thomas, J. M.; Thomas, W. J. "Introduction to the Principles of Heterogeneous Catalysis", 1st ed.; Academic Press Inc.: London, 1975; Chapter 2.
61. Sheppard, N.; James, D. I.; Lesiunas, A.; Prentice, J. D. Commun. Dep. Chem. (Bulg. Acad. Sci.) 1984, 17, 95-101.
62. Christmann, K. Bull. Soc. Chim. Belg. 1979, 88, 519-39.

APPENDIX

Substantial scatter is observed in Figures 13, 16 and 19 plotting methane rate versus an experimental variable. The methane partial pressures used in determining the rates are at very low, and their quantitation by gas chromatography with flame ionization detection is susceptible to interference from other gases. Ethylene elutes immediately after methane from the chromatographic column. At low ethylene pressures the difference of the retention times for methane and ethylene is small and the ethylene peak interferes with the methane peak. Likewise at high ethylene partial pressures the width of the ethylene peak results in strong interference with methane.

In Figure 13 the methane formation rate is plotted versus the hydrogen partial pressure. Hydrogen is not detected by the flame ionization detection directly but it can interfere with another gas eluting at the same time as seen in Figure 13. At high hydrogen partial pressures, methane detection is hindered by the hydrogen interference.

No conclusions of this thesis are based on Figures 13, 16 and 19. At the time these data were collected the primary purpose of the data collection was to determine the ethylene hydrogenation rate and the gas chromatograph was optimized with this in mind.